Engineered maleoyl-chitosan grafted with oligopeptides nanogels with dual-mode mobility toward melanoma therapy

Alina Gabriela Rusu[1]*, Loredana Elena Nițǎ[1], Alina Ghilan[1], Natalia Simionescu[2], Alexandru Mihail Șerban[1], Alexandra Vieru[1], Liliana Tarțău-Mititelu[3]

[1] Department of Natural Polymers, Bioactive and Biocompatible Materials, "Petru Poni" Institute of Macromolecular Chemistry, 41-A Grigore Ghica Voda Alley, Iasi, Romania

[2] Center of Advanced Research in Bionanoconjugates and Biopolymers, "Petru Poni" Institute of Macromolecular Chemistry, 41-A Grigore Ghica Voda Alley, Iasi, Romania

[3] Department of Pharmacology, Clinical Pharmacology and Algesiology, "Grigore T. Popa" University of Medicine and Pharmacy, Universităţii Street 16, Iasi, Romania

E-mail:

**Corresponding authors: Alina Gabriela Rusu, rusu.alina@icmpp.ro; tel.: +40758456190.*

Abstract

Melanoma is a particularly aggressive form of skin cancer, and existing conventional chemotherapies, such as dacarbazine (DTIC), tend to have poor selectivity and limited therapeutic efficacy. As a result, the development of advanced nanocarrier systems that combine magnetic guidance with enzyme-driven motion to enhance drug distribution and stability is a promising approach to address these challenges. In this study, self-assembled magnetic nanogels with dual-mode mobility composed of maleoyl-chitosan (MAC) grafted with oligopeptides containing leucine (Leu) and N-Carbobenzyloxy-lysine (Cbz-Lys) moieties via N-carboxyanhydride ring-opening polymerization and magnetic nanoparticles (MNPs) immobilized with glucose oxidase (GOx) were prepared and utilized as therapeutic systems for the delivery of DTIC. These nanosystems were characterized in terms of their structure, morphology, and colloidal stability. The GOx-MNP core-based nanogels had remanent magnetization for external magnetic guidance, as well as enzymatic propulsion in the presence of glucose, as confirmed by particle tracking assay. Mean square displacement (MSD) profiles revealed superdiffusive motion for all systems, which can potentially facilitate tissue penetration. The highest Cbz-Lys content increased the velocity up to 8.9 μm/s, attributed to the concentration gradient and surface interactions. *In vivo* assays confirmed good hemocompatibility and biocompatibility without adverse effects on the liver or kidney. DTIC-loaded nanogels demonstrated strong cytotoxicity against cancer cells while reducing toxicity to fibroblasts. Overall, this study presents a proof-of-concept platform that

utilizes glyco-oligopeptide nanogels combined with magnetic guidance and enzymatic-driven motility, aiming to improve drug penetration and delivery in melanoma therapy.

Introduction

Melanoma is by far the most common and aggressive malignancy in humans, with malignant melanomas having the highest incidence and limited response to conventional therapies (such as drug therapy, radiation therapy, and photodynamic therapy (PDT) [1]). However, these treatments have limitations, such as increased toxicity for normal cells, severe side effects due to radiation exposure in radiotherapy, and difficulty in targeting cancer tissue, especially in melanoma [2].

Despite the availability of numerous systemic therapies for the treatment of melanoma, dacarbazine (DTIC) continues to be the first-line treatment for metastatic melanoma in standard clinical practice [3]; DTIC is a long-standing FDA-approved chemotherapeutic agent for melanoma. However, it has a short half-life in the bloodstream, a low response rate and a limited clinical performance due to the hydrophilic and acidic nature of tumoral tissue, requiring administration of higher doses [3]. These issues often lead to drug resistance and non-specific toxicity to healthy host cells. Thus, these complications have generated significant interest in innovative nanotechnology-based drug delivery systems designed not only to improve drug stability, but also to facilitate local accumulation within tumour areas, and improve therapeutic outcomes for patients with melanoma [4].

To date, various nanocarrier-based strategies, including PEGylated liposomes, dendrimers, quantum dots, nano micelles, polymeric nanoparticles, nanogels and hybrid nanosystems [5] have demonstrated the potential to overcome the limitations of the traditional drug delivery methods by enhancing drug biodistribution and reducing systemic toxicity.

Among these nanocarriers, nanogels are an appealing class due to their good biocompatibility, high water content, low surface tension in biological environments, tunable network design, and ability to effectively encapsulate a wide variety of drugs, including both hydrophilic and hydrophobic compounds [6]. Nevertheless, due to the challenging tumour microenvironment, many reported nanogel systems have limited efficacy in solid tumors like melanoma, as they rely on passive diffusion and fail to penetrate dense tissues sufficiently [7, 8]. Moreover, imprecise nanogel architecture and poor surface chemistry often lead to aggregation, uncontrolled drug release, or reduced colloidal stability, all of which hinder their therapeutic use [6, 9]. Consequently,

rational architectural design approaches are necessary to improve structural stability and enhance the distribution of drug-loaded nanogels within the tumor. In this context, the chemical modification of natural polymers through oligopeptide grafting, combined with an active or guided transport mechanism, offers a rational approach to stabilizing the nanocarrier structure and introducing guided mobility within nanogel systems capable of improving intratumoral distribution.

Due to their essential biological properties like biocompatibility and biosafety, nanogels based on biopolymers are widely used in biomedical and pharmaceutical applications. Among these biopolymers, chitosan (Cs), a natural polysaccharide, has attracted great interest due to its versatile chemistry and functionalization potential. Cs is frequently used as a vehicle in drug delivery applications due to its improved biodistribution, increased specificity, environmental responsiveness, and reduced pharmacological toxicity. Moreover, due to the reactive groups (hydroxyl and amino groups) contained on its macromolecular chain, Cs can be functionalized with other compounds, which could confer desired properties to Cs-based materials [10, 11]. For example, by reacting maleic anhydride (MA) with the amino groups of Cs, a derivative with amphiphilic properties, namely maleoyl-chitosan (MAC), is obtained, which has a tendency to self-assembly with polyanions in nanogels and exhibits good solubility in organic solvents like DMSO or DMF. In a previously published work by our group, this Cs derivative was self-assembled with an anionic polypeptide (poly(aspartic acid)) to obtain nanogels that were subsequently encapsulated with amoxicillin to treat bacterial skin infections [12].

However, beyond this approach, further enhancement of interactions with ECM proteins and receptors and overall performance of nanogels can be achieved through the subsequent grafting of peptide segments or oligopeptides onto the Cs chain. This modification also allows for fine-tuning of amphiphilicity and promotes a more controlled self-assembly under physiological conditions. [13]. This process contributes to improving colloidal stability and efficient loading of chemotherapeutic agents [14], peptides, nucleic acids [15], and proteins [16], and adaptability in complex biological environments, such as tumors. More specifically, the inclusion of peptide or oligopeptide segments imparts additional properties, such as molecular specificity and the potential for cellular internalization by adsorption-mediated endocytosis [13].

In recent years, the integration of lysine (Lys) and leucine (Leu) residues in the construction of peptides such as L-K6 has attracted increasing interest in the field of nanomedicine due to their

ability to form stable self-assembled structures with cytotoxic specificity towards cancer cells by binding to DNA and inducing nuclear damage [17]. Leu, due to its hydrophobic character, contributes to self-assembly into nanostructures, while Lys, through its positive charges, supports colloidal stability through electrostatic interactions and induces potential responsiveness to biological environments [18, 19]. Moreover, using Lys in its carbobenzoxy-protected form (Cbz-Lys) can tune the peptide sequence polarity and decrease nonspecific interactions with serum proteins or other anionic components from the tumor microenvironment, while preserving the structural integrity of the self-assembled nanosystem [20, 21]. Based on these observations, grafting peptides/oligopeptides containing Leu/Lys residues onto the Cs backbone, a promising platform for advanced therapeutic applications and drug delivery can be obtained with enhanced colloidal stability, efficient drug loading capacity, biocompatibility and molecular specificity. Such derivatives with proven antimicrobial properties were obtained by Enright and collab. in which they used unmodified Cs to graft Leu and Lys [22]. Another research group used Cs modified with decanal on which they grafted 3,4-dihydroxyphenylalanine (DOPA), cysteine (Cys) and arginine (Arg). Instead, to obtain the polypeptide derivatives, the authors preferred to remove the decanal residues from the main chain of Cs to further develop a polymeric structure with applicability in hemostasis and soft tissue adhesions [23].

Despite the variety of conventional passive delivery systems, the non-uniform distribution of therapeutic agents remains one of the biggest challenges when it comes to solid tumors, making this type of delivery insufficient [24]. To increase the efficiency of drug delivery systems, recent research in nanomedicine has focused on solutions based on active or guided transport mechanisms capable of overcoming the barriers of the tumor microenvironment and improving intratumoral distribution [25, 26].

Among these, enzyme-driven systems, particularly those based on glucose oxidase (GOx), have attracted attention for their capacity to generate local chemical gradients in biologically relevant environments, facilitating the propulsion of nanocarriers [27]. In addition, magnetic nanoparticles also provide the potential for external guidance of carriers to the tumor sites, which is especially useful in melanoma treatment [28, 29]. Integrating these features into a single platform creates opportunities for improved control over drug delivery, adapted to the biological environment.

In this context, we developed a new type of hybrid nanogels based on chemically modified Cs grafted with oligopeptide segments and integrated with GOx-functionalized magnetic

nanoparticles for improved colloidal stability, selectivity and enhanced cytotoxicity toward tumor cells (melanocytes), while reducing toxicity to healthy cells (fibroblasts). These hybrid nanostructures are designed to encapsulate DTIC for melanoma treatment. In-depth focus is placed on understanding how oligopeptide composition influences not only nanogel formation, colloidal stability and morphology, but also drug loading and release, enzymatic activity, and motion behavior, while analyzing the limitations and potential of the proposed approach for melanoma therapy.

The novelty of the study relies on two aspects: first, the amphiphilic glyco-oligopeptides shell is anticipated to stabilize the nanocarrier structure and to facilitate the diffusion through cell membranes. Second, the core composed of GOx-MNPs will provide enzymatic activity for mobility while also allowing for precise magnetic guidance. This complex propulsion mechanism aims to improve the diffusion into tumor cells and provide accumulation of DTIC, overcoming the drawbacks of conventional passive delivery systems. To our knowledge, this study represents the first instance of developing gel-like nanocarriers with glyco-oligopeptidic outer shells and magnetically/enzymatically guided core, all aimed at improving the efficacy of melanoma therapy.

2. Experimental

2.1. Materials

Medium molecular weight chitosan (Cs) (degree of deacetylation = 75–85%, M_w = 190 000–310 000 g mol^{-1}), maleic anhydride (MA), L-leucine (Leu), triphosgene, glucose oxidase (EC 1.1.3.4) type II-S from Aspergillus niger (activity 18.2 U/mg), squaric acid, 4-aminoantipyrine (4-AAP), phenol, peroxidase from horseradish Type I (activity ≥50 units/mg solid), glucose, 3-(aminopropyl)-triethoxysilane (APTES, 99%) and dimethyl sulfoxide (DMSO), were purchased from Sigma Aldrich (Hamburg, Germany). Ferric chloride hexahydrate ($FeCl_3 \cdot 6H_2O$) and ferrous chloride tetrahydrate ($FeCl_2 \cdot 4H_2O$) were provided by Merck (Darmstadt, Germany) and dacarbazine (DTIC) by TCI Chemical (Zwijndrecht, Belgium). N^{ε}-carbobenzoxy-L-lysine (Cbz-Lys) was obtained from Acros Organics (Geel, Belgium). Tetrahydrofuran and hexane acquired from Sigma Aldrich (Hamburg, Germany) were utilized as organic solvents in the synthesis of N-carboxyanhydrides from Leu and Cbz-Lys. The ultra-high purity water used in the study, either

for synthesis reactions or characterization of the materials, was produced by a Milli-Q 7000 system (Merck Millipore; Burlington, MA, USA).

2.2. Obtaining Cs derivative grafted with oligopeptides

2.2.1. Modification of Cs with MA

A previously reported method was used to produce the Cs derivative (MAC) [30] with increased solubility in distilled water and DMSO. Using a molar ratio of 1/5 Cs/MA, the functionalization of Cs with MA was carried out in a 5% acetic acid solution, adding MA under mild stirring. The obtained Cs/MA mixture was stirred for 18 hours at room temperature. After dialysis, the solution was freeze-dried. Additionally, to prevent the polysaccharide from becoming O-acylated and to create partly acylated Cs, the Cs solution was diluted with methanol, a reactive O-nucleophile co-solvent.

To confirm the successful modification, the molecular weight (M_W) of the modified Cs derivative, namely MAC, was measured using static light scattering (SLS) as described thoroughlyin the Supplementary Information (Section S2). The results indicated an M_w of 24.4 kDa for MAC.

2.2.2. Synthesis of Leu-NCA and Cbz-Lys-NCA

The N-carboxyanhydrides of Leu and Cbz-Lys (Leu-NCA and Cbz-Lys-NCA) were prepared by the Fuchs-Farthing method (Fig. 1A) [31].

Briefly, Leu was transferred into a round-bottomed flask containing 10 mL of anhydrous tetrahydrofuran (THF); triphosgene (Leu/triphosgene molar ratio = 2:1) dissolved in anhydrous THF (10 mL) was added to the formed suspension and stirred at 50°C in an N_2 atmosphere. After 3 hours, Leu-NCA was precipitated with anhydrous n-hexane. The resulting white precipitate was then washed with a mixture of THF/n-hexane and dried at room temperature to give a white solid. Purification by recrystallization was repeated three times to ensure the removal of unreacted precursors and to guarantee the high purity of the resulting N-carboxylic anhydrides. The N-carboxyanhydride of Cbz-Lys was synthesized by a similar process, with the only difference being the molar ratio between the amino acid and triphosgene, which was 1:1.

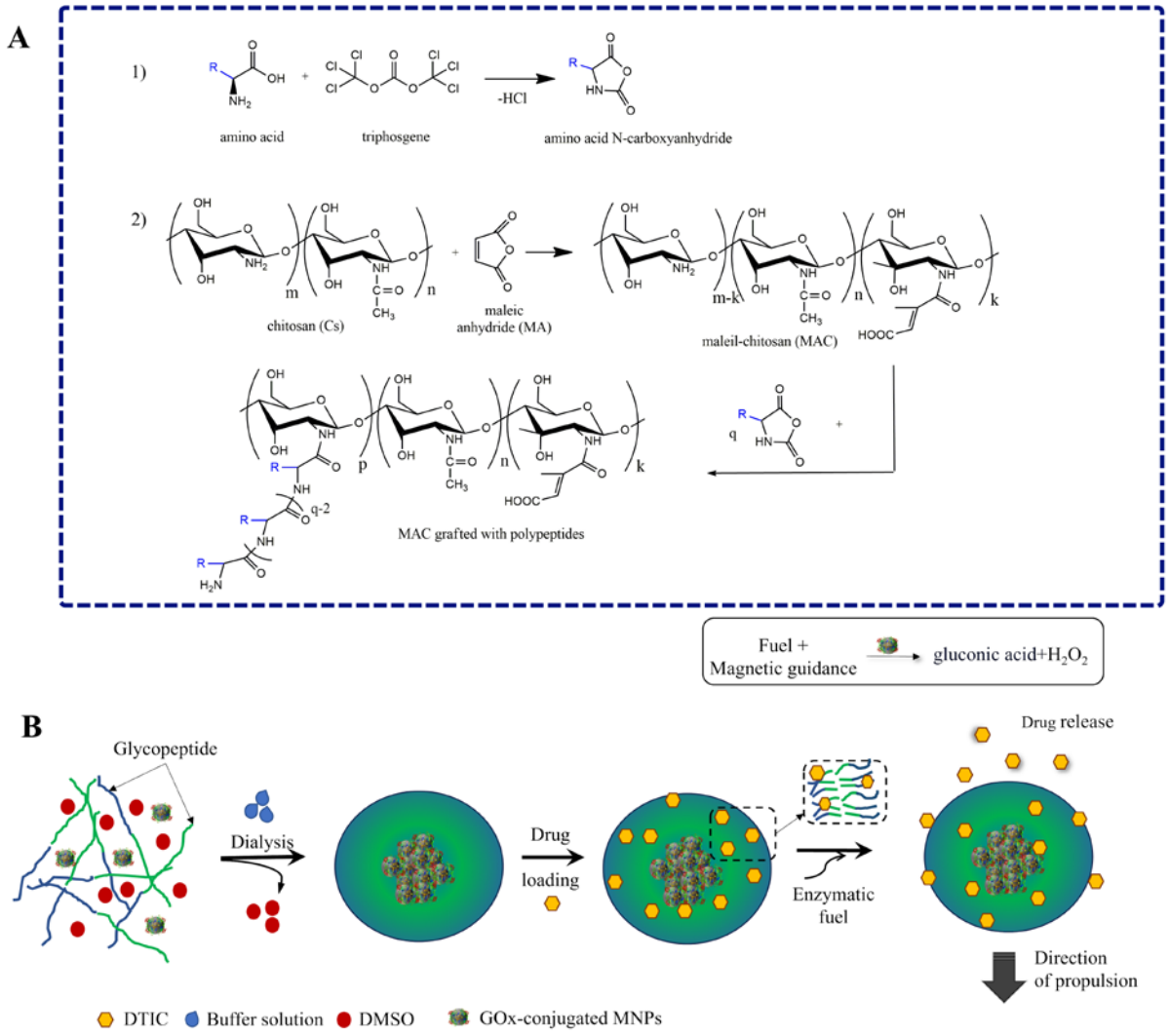

Fig. 1. A) Schematic representation of 1) Leu-NCA and Cbz-Lys-NCA synthesis and 2) grafting to MAC through ROP; B) Illustration depicting the self-assembly process of glyco-oligopeptides and GOx-MNPs.

2.2.3. Grafting of oligopeptides on Cs derivative

The MAC-grafted-oligopeptides preparation process consisted of the ring-opening polymerization (ROP) of the Leu-NCA and Cbz-Lys-NCA in the presence of MAC, used as a macroinitiator through the remaining unmodified amino groups (see Fig. 1A). One of the main reasons MAC is preferred as a backbone for glyco-oligopeptidess synthesis is due to its solubility in DMSO. Unlike native chitosan, which has limited solubility, MAC facilitates homogenous reaction conditions in DMSO. The improved solubility of MAC results from the substitution of Cs amino groups with

the MA radical, reducing inter- and intramolecular hydrogen bonding and enabling uniform grafting conditions during glyco-oligopeptide synthesis.

Before the reaction, the Cs derivative was dissolved in a mixture of DMSO and distilled water (volumetric ratio 9:1 v/v) under mild heating (40 ^{o}C), obtaining a homogenous solution, while both Leu-NCA and Cbz-Lys-NCA were dissolved in DMSO; the molar ratios between the reactants are presented in Table 1. After 20 hours at 50 °C, the resulting viscous liquid was precipitated by adding acetone and then washed with acetone three times. The compounds were dried under reduced pressure, redissolved in DMSO, and reprecipitated in cold acetone. The purification step was repeated three times to ensure efficient removal of unreacted NCA monomers or low-molecular-weight species.

By varying the feed ratio, as detailed in Table 1, different glyco-oligopeptides were obtained and the schematic representation of the preparation process of the glyco-oligopeptidess is shown in Fig. 1B. Furthermore, calculations based on the feed ratios presented in Table 1 and M_W of MAC revealed that the total monomer-to-initiator molar ratios used in the experiments were 2.0:1, 2.55:1 and 2.83:1. These correspond to theoretical average oligopeptide chain lengths of approximately 2.0, 2.5 and 2.8 oligopeptide residues.

Table 1. Composition of glyco-oligopeptide based on the utilized feed ratios.

Sample	Mass ratio (MAC:Leu-NCA:Cbz-Lys-NCA) (g/g)	NH_2 unreacted (mmol)	Leu-NCA (mmol)	Lys-NCA (mmol)	M:I (NCAs: unreacted NH_2) (mmol/mmol)	Molar Ratio Leu:Lys (mmol/mmol)	DP theoretical (units/graft)
ML	1:1:0	2.75	5.46	-	2.0:1	-	2.0
MLL0.5	1:1:0.5	2.75	5.46	1.55	2.55:1	3.52:1	2.55
MLL0.75	1:1:0.75	2.75	5.46	2.33	2.83:1	2.34:1	2.83

2.3. Synthesis of magnetic nanoparticles conjugated with enzymes with catalytic activity

To obtain the desired nanomaterials, the process began with the preparation of Fe_3O_4 magnetic nanoparticles (MNPs) using the conventional co-precipitation method, as described in the literature [32].

Following preparation, the surface of Fe_3O_4 MNPs was sequentially modified: first, with (3-aminopropyl) triethoxysilane (APTES) at a 4:1 molar ratio, and subsequently reacted with a 0.5% squaric acid solution under continuous stirring for 24 hours. After these modifications, the nanoparticles were washed with ultrapure water to prepare them for GOx immobilization.

The GOx-conjugated MNPs, intended to be used as the magnetic nanogels core, were synthesized and extensively characterized, and the obtained results were already included in a previously published article [33]. Next, the variant of MNPs presenting optimal colloidal stability in simulated biological solutions, namely those with an MNP/GOx ratio of 5:1, was selected for subsequent experiments.

2.4. Preparation of pristine nanogels and their encapsulation with MNPs conjugated with enzymes

All glyco-oligopeptidess were self-assembled using the dialysis nanoprecipitation method (composition ratios in Table 2). The solution of glyco-oligopeptides of specific concentration prepared in DMSO is filtered and then transferred into a dialysis membrane (mesh cut-off 3.5 kDa). After that, the membrane was immersed and dialyzed against around 100 mL of buffer solution (pH 6.5) while being gently stirred. During the first six hours, the dialysis solution was replaced every hour with brand-new, ultrapure water. Dialysis nanoprecipitation was carried out overnight, resulting in around 20 hours of exchange time. During this process, DMSO rapidly diffuses into the buffer solution compartment, leading to the aggregation of hydrophobic chains and the self-assembly process of amphiphilic glyco-oligopeptidess is initiated; the particles obtained from nanoprecipitation were investigated in relation to composition (the ratio between the peptide segments - Leu and Cbz-Lys) and the concentration of the glyco-oligopeptides. The nanosystems with good colloidal stability were chosen for the encapsulation of GOx-MNPs. Three ratios between glyco-oligopeptidess and MNPs were prepared (3:1, 4:1 and 5:1 g/g) and studied in relation to their colloidal stability in aqueous solution, and the obtained data are presented in Table S1 (see Supporting Information, Section S3). The proposed mechanism underlying the self-assembly of magnetic glyco-oligopeptides nanogels is presented in Fig. 1B, providing a visual representation of the process described above.

Table 2. Composition of glyco-oligopeptide-based polymers and magnetic nanogels after self-assembly.

Sample	Mass ratio MAC:NCA-Leu: NCA-Cbz-Lys (g/g)	Glyco-oligopeptides concentration (mg/mL)	Mass Ratio glyco-oligopeptides:MNPs (g/g)
ML	1:1:0	1	-
MLL0.5	1:1:0.5	1	-
MLL0.75	1:1:0.75	1	-
ML+ MNP(3:1)	1:1:0	1	3:1
MLL0.5+ MNP(3:1)	1:1:0.5	1	3:1
MLL0.75+ MNP (3:1)	1:1:0.75	1	3:1

2.5. Structural Characterization

A Vertex Bruker spectrophotometer (Ettlingen, Germany) was used to record the FT-IR spectra of the precursors and the freeze-dried hydrogels in transmittance mode. With 64 scans and a resolution precision of 4 cm^{-1}, the spectra of every compound were obtained at room temperature throughout the wave number range of 4000–400 cm^{-1}.

2.6. Morphological analysis

The magnetic nanogels were analyzed using scanning transmission electron microscopy (STEM) to determine their size and shape. The Verios G4 UC scanning electron microscope, equipped with a STEM 3+ detector from Thermo Scientific (Brno, Czech Republic), was utilized to register micrographs of the nanoparticles placed on carbon-coated copper grids. The analyses were conducted using an accelerating voltage of 30 kV and in bright-field mode. The ImageJ 1.48v analysis program was used to determine the average diameter of the polymeric nanoparticles.

Also, the pristine glyco-peptide nanogels were examined by TEM with a Hitachi High-Tech HT7700 electron microscope (Hitachi High-Technologies Corporation, Tokyo, Japan). A drop of solution was directly placed on a carbon-coated copper grid and allowed to dry before analysis. Due to the new high-resolution objective lens built into the apparatus, no staining was needed for

the sample preparation in this type of equipment. The current was 36 mA, and the operating voltage was 30 kV.

2.7. ^{1}H NMR spectroscopy for characterization of Cs derivatives

The chemical modification of Cs with MA (MAC) and the grafting of MAC with oligopeptides were examined using ^{1}H NMR spectroscopy. ^{1}H NMR spectra of Cs and MAC were carried out at a temperature of 80°C, in acidified D_2O (5 mg/mL) (the spectrum of Cs is presented in the Supplementary Information). In comparison, the oligopeptide-grafted Cs derivatives were dissolved in a binary mixture of 10% D_2O: 90% DMSO-d6 (5 mg/mL) at 25°C. To record all the spectra, a Bruker Avance DRX400 NMR spectrophotometer, Rheinstetten (Germany), with 16 scans and 0.1 Hz.

2.8. Dynamic Light Scattering (DLS) measurements of pristine/magnetic nanogels

The Malvern Zetasizer Nano ZS instrument (Malvern Instruments, UK) with a 4.0 mW He-Ne laser operating at 173° (back scatter mode) on 633 nm was used to measure the nanogels in water-based solutions (particle size, polydispersity). The Stokes–Einstein equation was used to calculate the hydrodynamic diameters from diffusion coefficients. Additionally, zeta potential (ZP) measurements were also performed with Malvern Instruments' ZetaSizer IV. Three separate tests were conducted on each sample at 25 ºC.

2.9. Magnetic susceptibility

Magnetic susceptibility was determined using the MSB – Auto magnetic susceptibility balance, manufactured by Geneq Inc., Ontario, Canada. The display on the balance shows either the volume susceptibility χV or the mass susceptibility χM, both of which are directly related to the volume or mass of the sample located in the measurement area of the balance.

2.10. GOx enzymatic activity assay

The GOx activity of the oligopeptide-grafted MAC nanogels with a GOx-MNPs core was tested by monitoring glucose oxidation using a modified Trinder colorimetric method, as previously reported by our group [33]. Initially, the pre-assay reagent was prepared by mixing horseradish peroxidase (500 U), 4-aminoantipyrine (4-AAP) (0.015 mmol), phenol (0.025 mmol) and glucose

(5 mmol) in 50 mL of phosphate buffer solution (0.1 M, pH 7.0). To initiate the enzymatic reaction, 2 mL of assay solution was mixed with 1 mL of a solution of magnetic nanogels and stirred for 30 s at room temperature. Moreover, solutions of precursors such as GOx-immobilized MNPs, free GOx of the same molar concentration and a control without enzyme were prepared and utilized to assess the influence on the overall enzymatic activity of the magnetic nanogels. In the case of the samples containing MNPs, after the reaction, the supernatant was separated using a semi-permanent magnet to ensure efficient removal of the nanoparticles before measuring the absorption. Finally, aliquots of the resulting supernatant were taken, and the absorbance was measured at 504 nm to determine the concentration of hydrogen peroxide (H_2O_2), reflecting enzymatic activity. Data analysis and graphing were performed using Origin 2018 SR1 software. The activity of the enzyme was determined by using Eq. (1) [34]:

$$Concentration\ of\ glucose\ \left(\frac{mg}{L}\right) = \frac{Abs\ (s)}{Abs\ (std)} \times C(g)(\frac{mg}{L}) \quad (1)$$

where *Abs(s)* is the absorbance of the sample, *Abs(std)* is the absorbance of the standard solution, and *C(g)* is the concentration of glucose in the sample.

2.11. Nanogels tracking assay analysis

The motion videos of the glyco-oligopeptide nanogels with a magnetic core in a 10 mM concentration of glucose solution, which is the average concentration in human blood [35] were acquired using a MICROS Austria microscope with a 40 × objective at a frame rate of 7 frames per second. Videos were analysed in terms of trajectories and speed using the software ImageJ and Tracker 6.3.1. The data obtained after detecting particle trajectories was used to calculate the time-averaged mean square displacement (MSD), which is the square of the net distance a particle travels, as a function of lag time, τ. For the MSD calculation, Eq. (2) from below:

$$MSD = \Delta r^2(\tau) = \frac{1}{N-n}\sum_i^{N-n}[(x_{i+n} - x_i)^2 + (y_{i+n} - y_i)^2] \quad (2)$$

where *Δr2(τ)* is the *MSD* at a lag time *τ*, *n* is the number of time steps between the initial and final position used in the MSD calculation, *N* is the total number of recorded data points, x_i and y_i represent the coordinates of the point (position in space) at time t_i and x_{i+t} and y_{i+t} are the coordinates of the same point after a time τ.

A log–log plot of MSD versus time is typically used to determine the type of motion described by the nanosystems, based on the slope values from the curves, specifically α. If the logarithmic slope values of the MSD (α) are close to 1, then the particles are characterized by Brownian motion; moreover, at a value of $\alpha < 1$, their movements correspond to subdiffusion, and if $\alpha > 1$, then we are dealing with a displacement characterized by superdiffusion [36].

2.12. Thermogravimetric analysis of magnetic nanogel's stability

Thermogravimetric analysis of the dried nanogels was performed using an online TG-DSC/FT-IR/MS system, which includes a model STA 449F1 Jupiter (Netzsch, Selb, Germany), FT-IR spectrophotometer Vertex-70 model (Bruker-Germany) and mass spectrometer QMS 403C Aëolos model (Netzsch, Selb, Germany). The samples were heated under nitrogen at a flow rate of 50 mL/min in an open Al_2O_3 crucible, with a heating rate of 10 °C/min from room temperature to 600 °C. Data collection was performed using Proteus® software.

2.13. In vitro enzymatic degradation tests

The *in vitro* degradation of nanoparticles was studied in the presence of lysozyme in a buffer solution of pH 7.4. In the biodegradation experiment, an adequate amount of lysozyme (c=0.1 mg/mL), similar to that used by other researchers to investigate the biodegradability of Cs-based nanosystems in physiological conditions, was added over the magnetic nanogels in the freeze-dried state (1.3 mg/mL) to initiate biodegradation. The catalytic process was evaluated at 37 °C by the DLS technique inside a glass cuvette to measure the *in situ* changes that D_h undergoes over time [37]. A comprehensive description of the results is available in the Supporting Information (Section S4).

2.14. Drug loading/release of DTIC

Although it is possible to include therapeutic compounds in nanogels during their formation, in this study, DTIC was encapsulated after the nanosystems had been obtained. This strategy aids in mitigating potential negative consequences on the carrier network [38], like increased polydispersity, reduction of colloidal stability, alteration/modification of surface properties, or excessive loading that leads to cytotoxicity. Thus, DTIC, the chosen drug, was encapsulated using

a shaker (magnetic nanogels: drug mass ratio 1.3:1 g/g) and the free drug was removed through magnetic separation. Following magnetic separation, the drug loading (DL) and encapsulation efficiency (EE) were assessed at 328 nm by UV-VIS spectroscopy, with calculations performed according to Eq. 3 and Eq. 4.

$$EE\ (\%) = \frac{initial\ amount\ of\ drug - amount\ of\ unloaded\ drug}{initial\ amount\ of\ drug} x100 \quad (3)$$

$$DL\ (\%) = \frac{amount\ of\ drug\ in\ nanoparticles}{amount\ of\ nanoparticles\ and\ drug\ taken\ for\ loading\ studies}\ x\ 100 \quad (4)$$

In a series of *in vitro* release experiments, the ability of magnetic nanogels to perform as an efficient controlled release vehicle for antitumoral drug delivery was investigated by monitoring the time dependence of DTIC release from the glyco-oligopeptides-based nanogels in phosphate buffer solutions with two different pH levels: one at pH 6.5, which is similar to the pH of the tumor extracellular microenvironment, and the other at pH 7.4, which is the normal physiological pH of non-cancerous cells via the dialysis method. Each magnetic nanogels batch loaded with DTIC was dispersed in a 2.0 mL phosphate buffer solution, immediately transferred to a dialysis membrane (Mn = 14000 Da) and dipped in the release medium (25 mL). At predetermined time intervals, 1.0 mL of the release medium was extracted to determine drug concentration by UV-VIS spectroscopy at specific wavelengths (λ_{DTIC} =328 nm) and replaced with 1.0 mL of new buffer solution. The measurements were performed in triplicate for each sample, and mean average values with standard error (±SD) were calculated.

2.15. Assessment of cytotoxicity of nanoparticles (MTS assay)

Normal dermal fibroblasts (NHDF, PromoCell, Heidelberg, Germany) and malignant melanoma cells (MeWo, CLS Cell Lines Service GmbH, Eppelheim, Germany) were cultured in alpha-MEM medium (Lonza, Basel, Switzerland) supplemented with 10% serum fetal bovine (FBS, Gibco, Thermo Fisher Scientific, Waltham, MA, USA) and 1% penicillin-streptomycin-amphotericin B mixture (10 K/10 K/25 μg, Lonza, Basel, Switzerland).

Cytotoxicity of ML_MNP (3:1), MLL0.5_MNP (3:1) and MLL0.75_MNP (3:1) and of those loaded with DTIC (ML_MNP (3:1)_DTIC, MLL0.5_MNP (3:1)_DTIC and MLL0.75_MNP (3:1)_DTIC) was determined by the MTS technique using the CellTiter 96® AQueous One Solution Cell Proliferation Assay kit (Promega, Madison, WI USA), according to the

manufacturer's instructions. Cells were seeded in 96-well cell culture plates at a density of 0.6 × 10^5 (NHDF) or 1.2 × 10^5 cells/mL (MeWo). The next day, the cells were incubated for 24h with 100 µl fresh complete medium (Control), different concentrations of nanoparticles (NPs) or different concentrations of DTIC (Table 3), equivalent to the concentrations loaded in the NPs. After 21h, 20 µL MTS reagent/well was added, and the absorbances were measured after 3h at a wavelength of 490 nm using a FLUOstar® Omega microplate reader (BMG LABTECH, Ortenberg, Germany). The experiments were performed in triplicate, and the viability of the treated cells was expressed as a percentage of the viability of the Control cells. Data plotted were expressed as means ± standard error of the mean.

Table 3. Magnetic nanogels and DTIC concentrations used in cell culture experiments.

Sample	NP (µg/mL)	DTIC (µg/mL)
ML+MNP (3:1)	175	0
MLL0.5 + MNP(3:1)	233	0
MLL0.75+ MNP (3:1)	292	0
ML+MNP (3:1)_DTIC	175	150
MLL0.5 + MNP (3:1)_DTIC	233	200
MLL0.75 + MNP (3:1)_DTIC	292	250
DTIC	0	150
	0	200
	0	250

2.16. Assessment of acute toxicity and biocompatibility in vivo

The experiment used white Wistar rats (3 months old), healthy, not genetically modified, weighing 150-200 g, with a uniform gender distribution (half male, half female), which were purchased from the National Institute Medical-Military "Cantacuzino" for Research and Development, Baneasa Station, Bucharest, Romania and brought to the biobase of the "Grigore T. Popa" University of

Medicine and Pharmacy, Iasi from the CEMEX laboratory ("Advanced Center for Research and Development in Medicine experimental - CEMEX").

For acute toxicity and *in vivo* biocompatibility testing, 3 batches of 6 animals each were used, which received the substances subcutaneously, in a single dose, according to the following protocol:

Batch I (coded M): distilled water 0.15 mL/100 g body - control;

Batch II (coded ML): the sample containing nanogels without MNPs

Batch III (coded ML+MNP (3:1)): the sample containing polymers with MNPs covered with GOx

The acute toxicity and biocompatibility testing of the compounds were based on the investigation of the hematological, biochemical and immunological profile of the animals that received the test substances.

The biocompatibility evaluation was performed on blood samples collected from the lateral tail vein of the tested animals (0.5 mL) after general anaesthesia with 1% isoflurane. From the collected samples, hematological and biochemical determinations were carried out (on special analyzers), determining: the number of erythrocytes (GR), the values of hemoglobin (Hb) and hematocrit (Ht), the leukocyte formula, the activity of liver enzymes (alanine aminotransferase - ALT, AST - aspartate aminotransferase, lactate dehydrogenase - LDH), serum level of urea and creatinine, immune parameters (serum complement, phagocytosis capacity of polymorphonuclear neutrophils from peripheral blood - Nitroblue tetrazolium test - NBT, C3 and C4 fractions of complement), serum level of interleukin 6 (IL-6) and the value of tumor necrosis factor alpha (TNFα).

The evaluation of serum complement activity was performed using the Hartmann-Brećy technique, the principle of which is based on the hemolysis of sensitized erythrocytes (containing specific antibodies) by serum complement. It is considered that a percentage of 50% hemolysis provides much more accurate information about the activity of the complement in the blood, than total hemolysis.

The NBT test (with the percentage expression of the phagocytosis capacity of PMN from the blood) allows the identification of metabolic changes that occur during the phagocytosis processes, in direct correlation with phagocytosis, based on the reduction of nitro blue tetrazolium.

These blood parameters were determined using the HemaVet 950FS veterinary hematology analyzer (Drew Scientific, Inc., Boston, United States) and the VITROS 750 XRC biochemical test analyzer (Alphasoft, Bochum, Germany), using specific reagents from the company Johnson & Johnson (Johnson, New Haven, United States).

2.17. In vitro hemocompatibility investigation

For the standard hemolysis test, 0.2 mL of fresh blood was collected from the lateral tail vein of laboratory animals in vacutainers with heparin and mixed with sterile physiological serum in a ratio of 4 : 5. Sterile physiological serum was used as a negative control and Triton X-100 10% (v/v), known to possess hemolytic activity, incubated for 45 minutes at 37˚C, was considered as a positive control in the experiment. 0.2 mL of extraction medium from each sample was incubated in a water bath at 37°C for one hour. Then, each tube was centrifuged for 10 minutes at 1,000 RCF (Relative Centrifugal Force), and then the absorbance of the supernatant was recorded at a wavelength of 545 nm, using a Hewlett Packard 8453 UV–VIS spectrophotometer (Waldbronn, Germany). The percentage of hemolysis (% hemolysis) was calculated using the following Eq. 5 [39]:

$$\%\ hemolysis = \frac{(A_{tested\ substante} - A_{negative\ control})}{(A_{positive\ control} - A_{negative\ control})} \times 100 \quad (5)$$

where $A_{tested\ substance}$ is the absorbance of the tested substance, $A_{negative\ control}$ is the absorbance of the negative control, and $A_{positive\ control}$ is the absorbance of the positive control.

The complete data analysis is provided in Supporting Information, Section S6.

2.18. Statistical Analysis

All the investigations were carried out in triplicate, and the results are presented as mean ± standard deviation (S.D.).

Statistical analyses were conducted for both *in vitro* and *in vivo* experiments that required group comparisons. For the *in vivo* assays, these evaluations were performed using SPSS software (version 24.0, IBM, Armonk, NY, USA) and MATLAB's Statistics Toolbox (version 9.8.0, R2020a; The MathWorks, Natick, MA, USA). Group comparisons were analyzed using one-way ANOVA, following the assessment of data distribution with appropriate normality tests. Statistical

significance was defined as a p-value less than 0.05 when compared to the control group. In addition, for *in vitro* cytotoxicity, group comparisons at the same concentration were realized using a two-tailed Student's t-test (n = 3, dl = 4).

For the physicochemical characterization (including DLS measurements, drug release, enzymatic degradation), no additional statistical comparisons were conducted.

2.19. Research Ethics

The *in vivo* procedures were performed in alignment with recognized ethical standards for animal experimentation, following formal approval granted by the Ethics Committee of "Grigore T. Popa" University of Medicine and Pharmacy in Iaşi (Certificate No. 24/14.07.2020). All experimental protocols conformed to relevant national legislation and international guidelines, including Directive 2010/63/EU of the European Parliament and Council concerning the welfare and protection of animals used for scientific research [40].

3. Results and discussion

3.1. Characterization of Cs derivative grafted with oligopeptides

3.1.1. Structural characterization of the functionalized polysaccharide grafted with oligopeptides

Spectral analysis (FT-IR)

To highlight the structural modification, Fig. 2A and Fig. 2B show the FT-IR spectra of MAC, Leu-NCA, Cbz-Lys-NCA and derivatives grafted with oligopeptides (ML, MLL0.5 and MLL0.75). In the FT-IR spectrum of MAC, not only were characteristics peaks of Cs present, but also new peaks, confirming the functionalization with MA as previously described [41]: an intense broad band around 3400 cm^{-1} attributed to the stretching of −NH and hydrogen-bonded −OH, at 2900 cm^{-1} a low-intensity band ascribed to the stretching of −CH, at 1630, 1540, and 1454 cm^{-1} corresponding to the regions of amide I (C-O stretching), amide II (low-intensity NH bending) and amide III (C−N stretching and NH in-plane deformation), respectively.

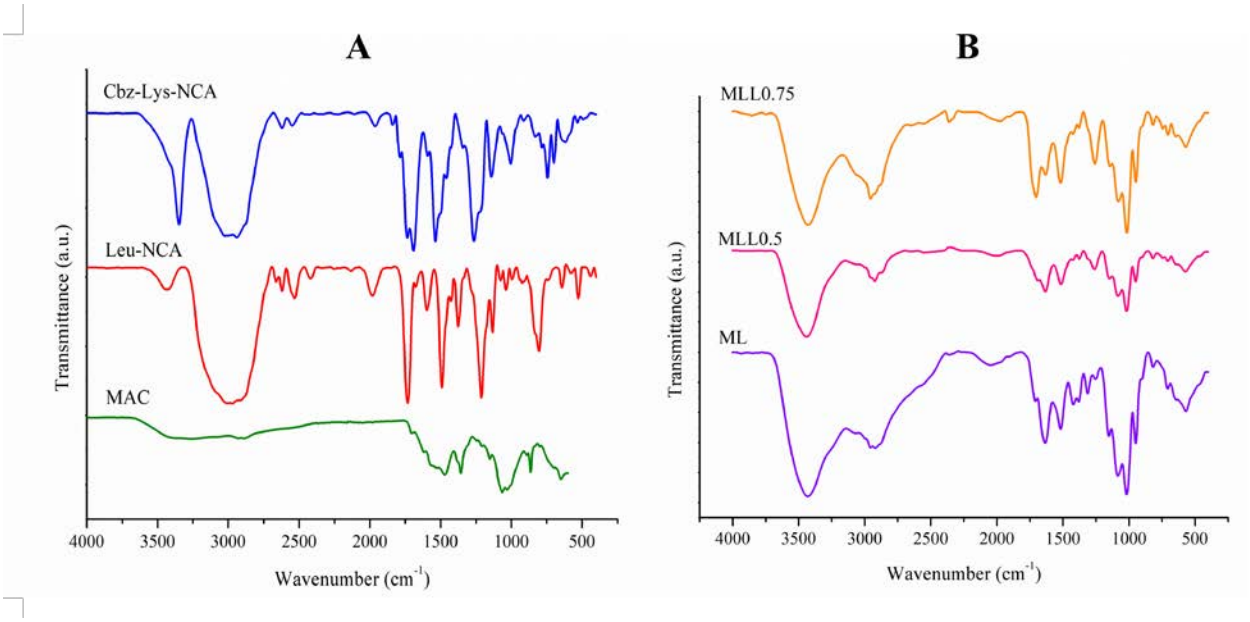

Fig. 2. Spectral characterization of Cs derivative grafted with oligopeptides. A) FT-IR spectra of MAC, Leu-NCA, Cbz-Lys-NCA; B) FT-IR spectra of ML, MLL0.5 and MLL0.75 compounds.

The IR spectra of Leu-NCA/Cbz-Lys-NCA compounds present absorption bands at 1738 cm^{-1} and 1694 $cm^{-1,}$ which are attributed to the asymmetric $NH(C=O)_2O$ stretching vibration and amide C=O stretching vibration of the N-carboxylic anhydride [42, 43]. The additional distinctive peak occurring around 3400 cm^{-1} is attributed to the N-H stretching (amide and Lys side chain amine), and specifically for the Cbz-Lys-NCA compound, the peak from 3025 cm^{-1} is linked to the stretching of aromatic C-H from the Cbz side chain. In the case of the ML compound obtained after MAC grafting with Leu-NCA, the absorption bands specific to the asymmetric and symmetric C=O stretching vibrations of the N-carboxylic anhydride were not recorded in its IR spectrum, indicating the consumption of Leu-NCA precursor. The same observation is valid for the other two glyco-oligopeptidess, MLL0.5 and MLL0.75. In addition, the IR spectra of MAC conjugated with oligopeptides reveal characteristic pLeu/p(Cbz-Lys) peaks [44, 45], such as those specific to the carbonyl group from the amide I (C=O stretching) and amide II (N-H bending and C-N stretching) of the peptide bond, approximately at 1630 cm^{-1} and 1510 cm^{-1}, respectively, confirming the ROP of precursors and grafting to MAC. In addition, the absorption band in the domain 3200-3400 cm^{-1} is attributed to the stretching vibration of the amide N-H bonds.

Nuclear magnetic resonance spectroscopy (^{1}H NMR)

The degree of modification of Cs with MAC (48.12%) was quantified via ^{1}H NMR spectroscopy by comparing the integral ratios of signals assigned to the protons in the ethylene group (MA moieties) and H2 from the glucosamine backbone of Cs (Fig. S1, Supplementary Information). Full spectra of Cs and MAC, peak assignments, and calculations are provided in the Supplementary Information.

The successful ROP of NCA and grafting of the peptides to MAC were validated by distinctive chemical shifts and characteristic peaks seen in the ^{1}H NMR spectra (Fig. 3, Fig. 4). In the case of MLL0.5 and MLL0.75, which contain both Leu and CBZ-Lys, the NMR spectra showed many characteristic peaks. Signals at 7.2–7.3 ppm indicated the presence of aromatic protons from the Lys protected by Cbz. The signals around 8.2 ppm in the ^{1}H NMR were associated with the grafting sites on the Cs derivative and the amide linkages in the peptide backbone. Moreover, the multiplets occurring at 3.5–3.7 ppm confirmed the presence of α-protons from Leu and Cbz-Lys residues. The protons in the β- and γ-CH_2 aliphatic side chains of Leu and Cbz-Lys exhibited peaks within the 1.5-1.8 ppm range.

In addition, the γ-CH_3 protons from the isopropyl group of Leu were identified as doublets appearing around 0.8 ppm. Moreover, specific peaks corresponding to Cs and its functionalization with MA were identified: H1 protons (δ= 4.5 - 5 ppm), H2 (δ=3.1 ppm), saccharidic ring hydrogen atoms (H3-H6) (δ= 3.4 – 3.86 ppm) and methyl group of –NHCO$\underline{CH_3}$ (δ= 2.0 ppm) from *N*-acetyl-D-glucosamine unit and protons from the ethylene group ((-HC=CH) of MA ((δ= 6.3-6.5 ppm).

Beyond signal identification, ^{1}H-NMR spectroscopy also allowed the estimation of the oligopeptide composition and the grafting density (number of Leu and Leu/Cbz-Lys units per acetylated MAC units) of the resulting MAC-graft-oligopeptide copolymers, based on the acetylmethyl protons of the Cs derivative (δ= 2.0 ppm). This type of measurement is similar to a previously described study for the synthesis of the chitosan-graft-polylactide, where the ratio of the signals mentioned above led to a quantification of the grafting density by the ^{1}H NMR technique [46]. Also, it should be noted that the grafting density values obtained from ^{1}H-NMR spectra represent averages, and they do not provide information regarding the distribution of chain-lengths.

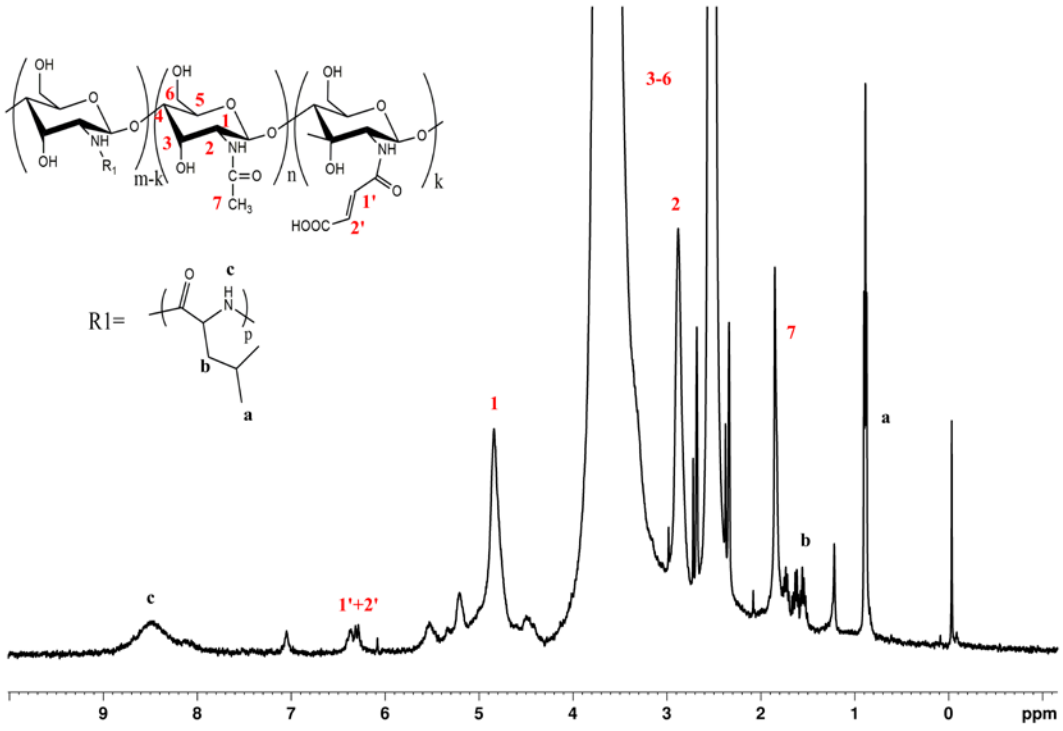

Fig. 3. ^{1}H NMR spectrum of ML.

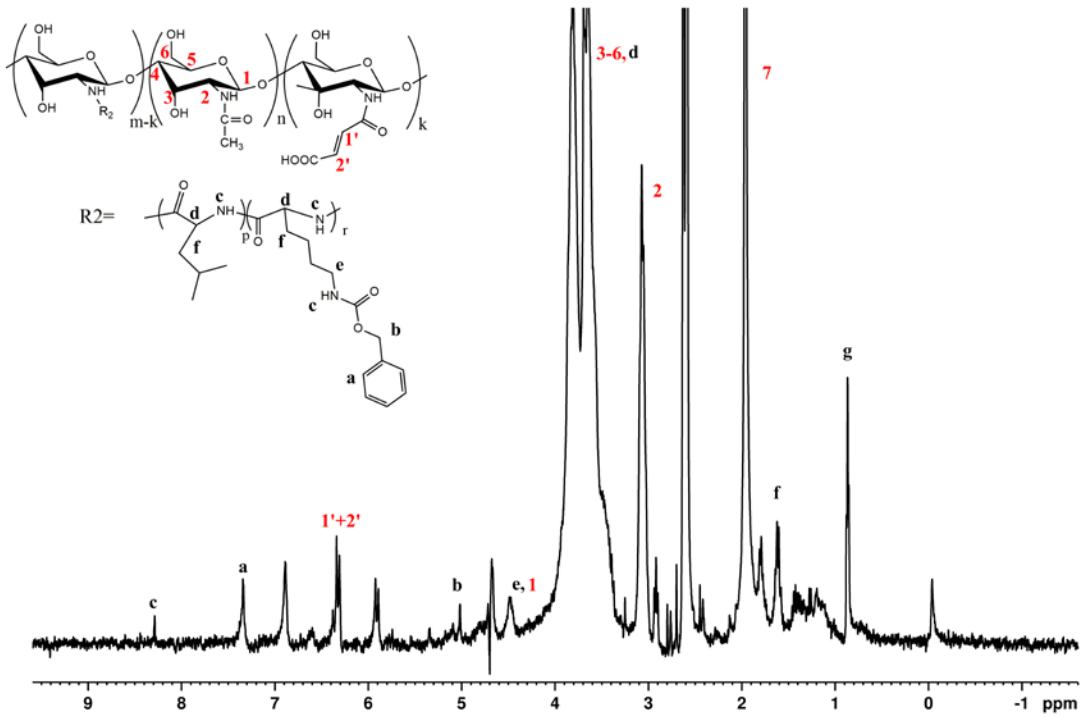

Fig. 4. ^{1}H NMR spectrum of MLL0.5.

By integrating the Leu methyl groups and the acetyl groups for the ML graft copolymer (without the Lys unit), a grafting density of approximately 11.6% was obtained, corresponding to a single Leu residue per grafted chain (DP ≈ 1.0).

For MLL0.5 (Leu-NCA + Cbz-Lys-NCA at a mass ratio of 1:0.5), there was a total grafting density of 7.7% for all MAC units, and the Leu/Lys molar ratio was 2.6:1, which corresponded to a peptide composition of approximately 73% leucine and 27% lysine, with an average peptide chain length of approximately 0.69 residues per graft per chain.

For MLL0.75 (Leu-NCA/Cbz-Lys-NCA at 1:0.75), the ¹H-NMR spectrum showed an estimated graft density of approximately 9.2% and an average peptide chain length per graft site of 0.80 residues per chain. The estimated graft composition was around 63% leucine and 37% lysine, at a Leu/Lys molar ratio of 1.68:1. These results confirm the formation of short oligopeptide side chains with tunable composition and density, depending on the NCA mass ratio.

Another observation was that the average oligopeptide chain length, as estimated from ¹H-NMR peak integration, was found to be 2–3 times that of the initial reaction feed (monomer-to-initiator molar ratios), which can indicate that a steric hindrance may be limiting chain growth. The lengths of the oligopeptide chains ranged between 1.0 and 0.69, which are suitable for both the self-assembly of glyco-oligopeptides into nanogels and for preserving the ability of the nanogels to disperse easily and their stability in aqueous environments. As reported in the literature regarding the design of nanocarriers [47], the presence of short oligopeptide side chains can contribute to the amphiphilic self-assembly process, which otherwise, longer chains can hinder the process [48].

3.1.2. The influence of glyco-oligopeptides composition and concentration on the self-assembly process

The evaluation of the size of nanogels is important for meeting various requirements imposed by medical applications. The ability to assemble was studied as a function of the concentration and composition of the peptidic segment to ensure not only the encapsulation of therapeutic agents in the glyco-oligopeptides shell, but also to maintain its stability when MNPs conjugated with enzymes are included. The average particle size distribution (Z-average) and ZP of the polymers

were measured, and the obtained data are presented in Table 4 below and Table S1 in Supporting Information, Section S3.

Table 4. Characteristics obtained during DLS determinations for glyco-oligopeptide-based polymers and magnetic nanogels after self-assembly

Sample	Z-average (nm)	PDI	ZP (mV)
ML	195	0.17	+17.0
MLL0.5	342	0.26	+8.5
MLL0.75	359	0.31	+8.0
ML+ MNP(3:1)	203	0.18	+19.0
MLL0.5+ MNP(3:1)	327	0.134	+7.68
MLL0.75+ MNP(3:1)	290	0.128	+7.45

At higher ratios of MAC to Leu-NCA (such as 5:1) (Table S1 and Table 3), the self-assembled polymers have a less charged and less stabilized surface, as evidenced by the ZP values that decrease from +17 to +11.7 with increasing mass ratio from 1:1 to 5:1. This indicates a clear trend: as the amount of Leu-NCA decreases relative to MAC, the ZP of the resulting nanogels decreases, leading to reduced surface charge. In change, an increasing ratio of Leu-NCA results in higher surface charge density and increased ZP, as observed in Table 4. These findings are due to interactions between the oligopeptide chains and the macromolecular backbone of MAC, which alter the structure and morphology of the nanoparticles.

To study the influence of the glyco-oligopeptide concentration on the assembly capacity, the ML compound with an MA: NCA-Leu ratio of 1:1 was selected. Thus, the effect of the compound concentration on the size of the particles formed by dialysis in buffer solution (pH 6.5) was investigated at the following concentrations: 0.1, 0.5, 1.0 and 2.0 mg/mL (Fig. 5A). The values of the average dimensions of the nanoparticles showed significant changes with the decrease in the concentration (Table S1 and Table 3).

DLS studies showed that the average hydrodynamic diameter (D_h) of the nanogels without MNPs decreased with the initial concentration of the glyco-oligopeptide, from 404 nm at 0.10 mg/mL (bimodal distribution) to 259 nm for 1.0 mg/mL (monomodal distribution). The ZP of the nanogels increased proportionally with the ML compound concentration from +10 to +25 mV, showing that the surface charge of the nanogels is increasing. Thus, the ZP values reported in Table S1 from Supplementary Information indicated a variable shielding effect on the surface charge depending on the concentration of the glyco-oligopeptidess. This variation was attributed to the different conformations adopted by the glyco-oligopeptides macromolecular chains in the buffer solution. Therefore, in dilute solutions the intermolecular interactions are weaker, thus allowing the shielding of the deprotonated groups with Na^+ ions through weaker interactions with the solute molecules (buffer solution).

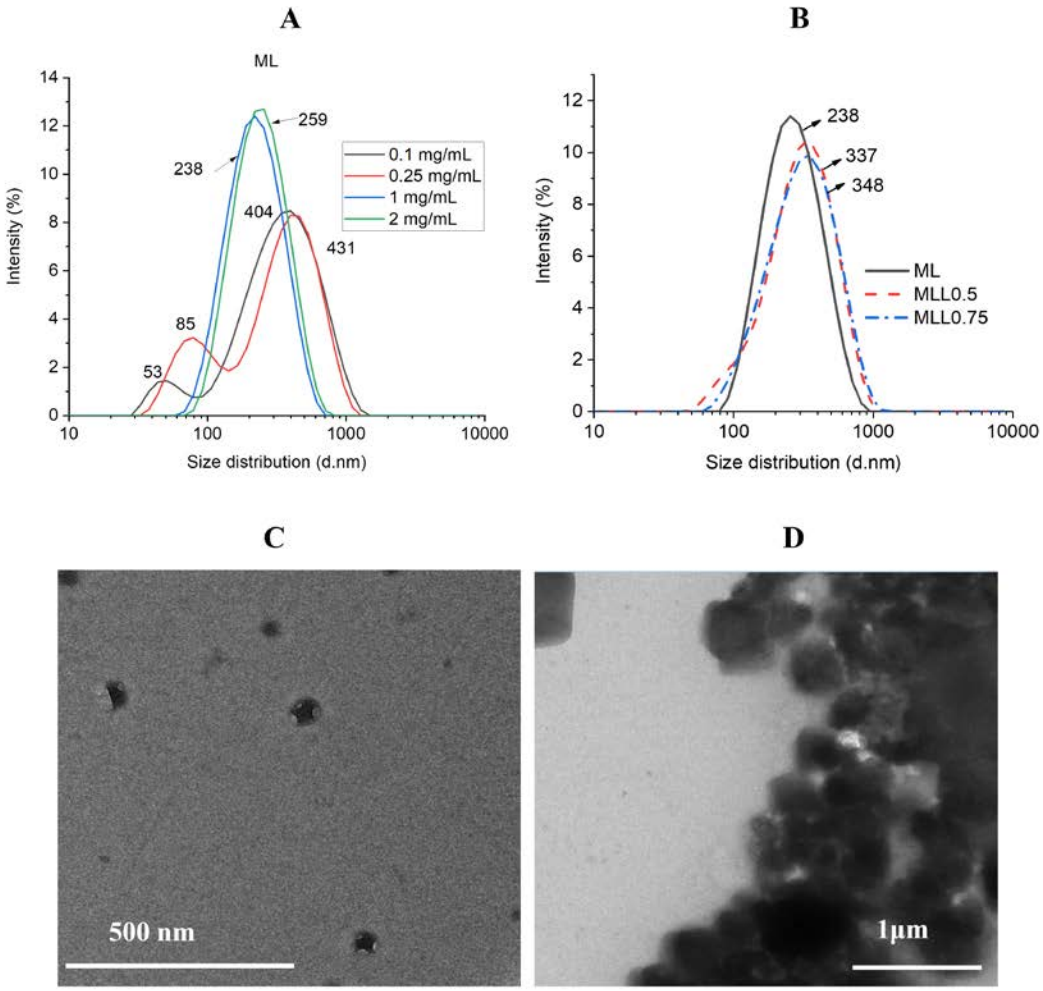

Fig. 5. A) Size distribution of nanoparticles assembled from glyco-oligopeptidess based on MAC/poly(leucine) at various concentrations; B) Size distribution of the self-assembled glyco-oligopeptidess (concentration 1mg/mL) based on ML, MLL0.5 and MLL0.75; C) TEM images of ML nanogels; D) TEM images of MLL0.5 nanogels.

Also, the DLS measurements on glyco-oligopeptides solutions with the peptide chain consisting of oligo(Leu-co-Cbz-Lys) in mass ratio 1/0.5 or 1/0.75 (Fig. 5B) demonstrated the formation of narrowly disperse structures, D_h varying from 337 to 348 nm, with PDI at a value around 0.3. Thus, increasing the Cbz-Lys content in the peptide chain leads to a slight increase in the nanogel size, as indicated by the higher D_h values. These observations can be explained by the increased hydrophobic and π-π interactions introduced by the aromatic groups contained in the Cbz radical. Although the overall degree of grafting slightly decreases (from 11.6% to 9.2%) with increasing the initial Cbz-Lys content, the presence of hydrophobic Lys derivatives leads to interchain association, thus reducing the surface charges and electrostatic stabilization, reflected by the decrease in ZP from +17 to +8. This change in the amphiphilic equilibrium probably leads to the formation of nanogels with larger dimensions and slightly increased PDI.

3.1.3. Transmission Electron Microscopy (TEM)

TEM images of the glyco-oligopeptides-based nanogels are shown in Fig. 5C and Fig. 5D and illustrate the morphology of the self-assembled systems. However, as can be observed from Fig. 5D, the glyco-oligopeptide nanogels aggregated upon diversification of the oligopeptide chains by the addition of Cbz-Lys. The increased size and tendency to aggregate are most likely due to hydrophobic interactions on the surface of the nanogels. Quantitative analysis using ImageJ software revealed that the average diameters of ML and MLL0.5 nanogels (1 mg/mL) are approximately 103 nm and 293 nm, respectively, supporting the observed trends in size variation. These diameters are smaller than those reported in the DLS study, likely due to the fact that electrostatic interactions between the charged polymers in solution cause a latency in the distribution of the diffusion coefficients during the DLS study. Thus, the observed morphology in TEM images may result from kinetic trapping caused by the rigidity of the oligopeptide segments, further influencing the assembly process of the nanogels. These observations are consistent with previous reports in the literature where spherical nanogels based on silk peptide and hyaluronic

acid were also obtained through dialysis against deionized water [49], supporting the reliability of our approach.

3.2. Characterization of nanogels encapsulated with MNPs conjugated with enzymes

3.2.1. The influence of the ratio between the glyco-oligopeptides and MNPs on the colloidal stability of the magnetic nanogels

Starting from the optimal concentration of 1mg/mL, three glyco-oligopeptides/MNP mass ratios (3:1, 4:1 and 5:1) were prepared for each Cs derivative: ML, MLL0.5 and MLL0.75. The DLS analysis of the glyco-oligopeptidess/MNPs systems showed particle sizes ranging from 194 nm to 336 nm and monomodal size distribution, confirming the two components were assembled into nanogels in buffer solution (Table 3 and Table S1). Likewise, no differences were recorded between the measured ZP values for each glyco-oligopeptides/MNPs ratio.

3.2.2. The influence of glyco-oligopeptides composition on the colloidal stability of magnetic nanogels in relevant biological media

For the MNPs systems coated with glyco-oligopeptidess, those containing MLL0.5 or MLL0.75 showed higher average size values (290 nm - 336 nm) as a result of the introduction of another amino acid (Cbz-Lys) in the formation of the oligopeptide chain, as well as a lower ZP (+7.26 mV - +7.68 mV) in comparison with the samples based on ML (Table 3).

This behaviour was attributed to the addition of N-blocked Lys with Cbz, which introduces supplementary physical interactions between the oligopeptide chains and the MAC macromolecular backbone. These interactions influence the assembly process, causing the arrangement of hydrophobic oligopeptide chains on the surface of the nanoparticles which in turn shields the surface charges and leads to a decrease in the ZP values.

The colloidal stability of the magnetic nanogels was evaluated at pH 6.5 (see Fig. 6), corresponding to slightly acidic, tumor-like conditions, and DLS measurements performed over a week did not reveal any significant variation in hydrodynamic diameter or PDI, indicating that the glyco-oligopeptide network of which the nanogel is composed maintains its structural integrity under biologically relevant conditions. Similarly, analysis of colloidal stability in DMEM confirmed that

the magnetic nanogels maintained good stability, with no formation of agglomerates that could inhibit cell proliferation (Fig. 6).

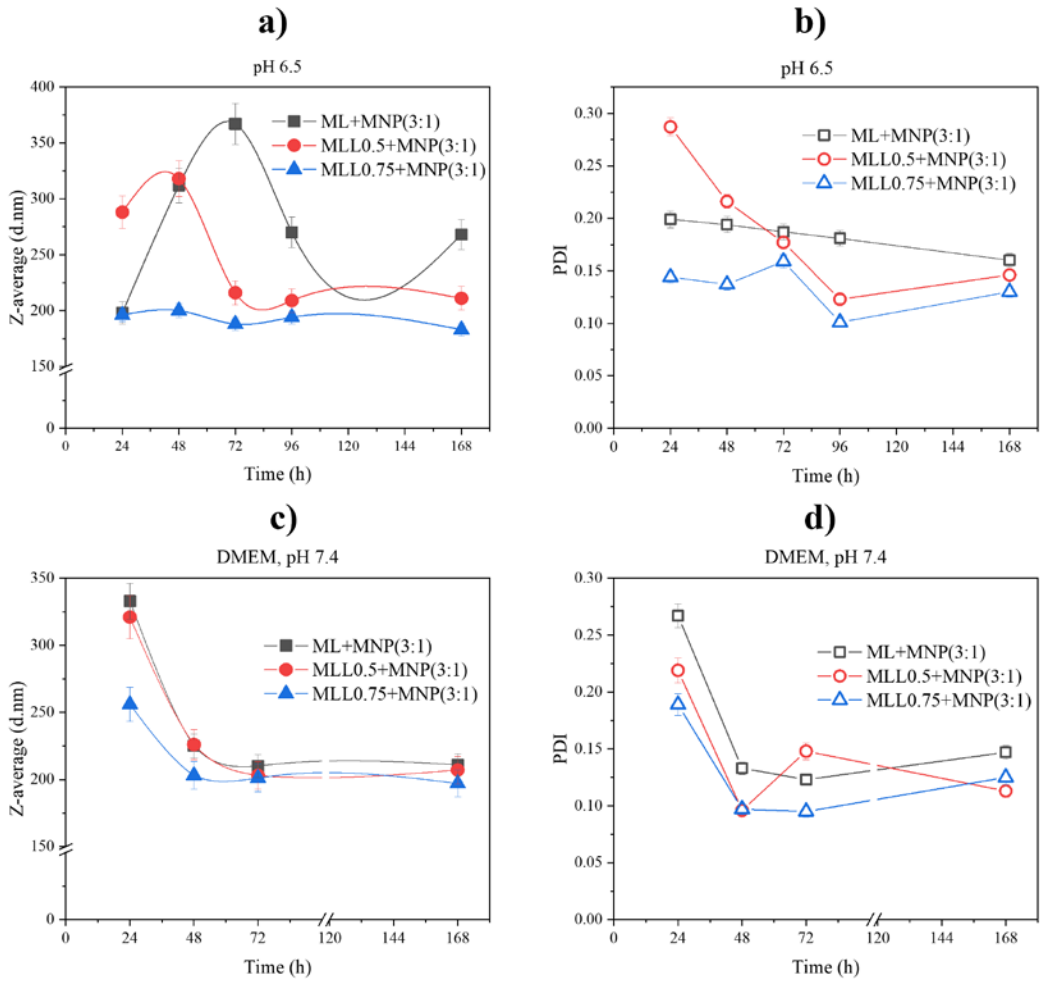

Fig. 6. Z-average and PDI of magnetic nanogel in a),b) PBS with pH 6.5 and in c), d) DMEM of pH 7.4.

Given that the colloidal stability analyses revealed no significant differences between the three used ratios, variants of magnetic nanogels with a 3:1 glyco-oligopeptides/MNPs ratio will be used for further studies, as these formulations have a good balance between stability and composition.

3.2.3. Structural analysis (FT-IR)

The FT-IR spectra of the glyco-oligopeptides/MNPs systems (Fig. 7) also showed absorption bands characteristic of the Cs modified with MA (MAC): stretching vibrations of the –OH group superimposed with the stretching vibrations of the N-H bond – range 3500 – 3400 cm^{-1}, C-H stretching vibrations at 2922 cm^{-1}; the stretching vibrations of the carbonyl group C=O at 1691 cm^{-1} and of the C-O bond in -COH- in the range 1078 - 1018 cm^{-1}.

In comparison to the spectra of glyco-oligopeptidess, the FT-IR spectra of magnetic nanogels presented absorption bands characteristic of the stretching vibration of amide I from peptide bonds. These bands appear at 1655 cm^{-1}, 1651 cm^{-1} and 1633 cm^{-1} for the samples ML+MNP (3:1), MLL0.5+MNP (3:1) and MLL0.75+MNP (3:1), respectively, confirming the presence of glyco-oligopeptidess in the composition of magnetic nanogels.

Also, the absorption band specific to the Fe-O bond is observed in all spectra of the magnetic nanogels at 559 cm^{-1} for ML+MNP (3:1), 523 cm^{-1} for MLL0.75+MNP (3:1) and 521 cm^{-1} MLL0.75+MNP (3:1).

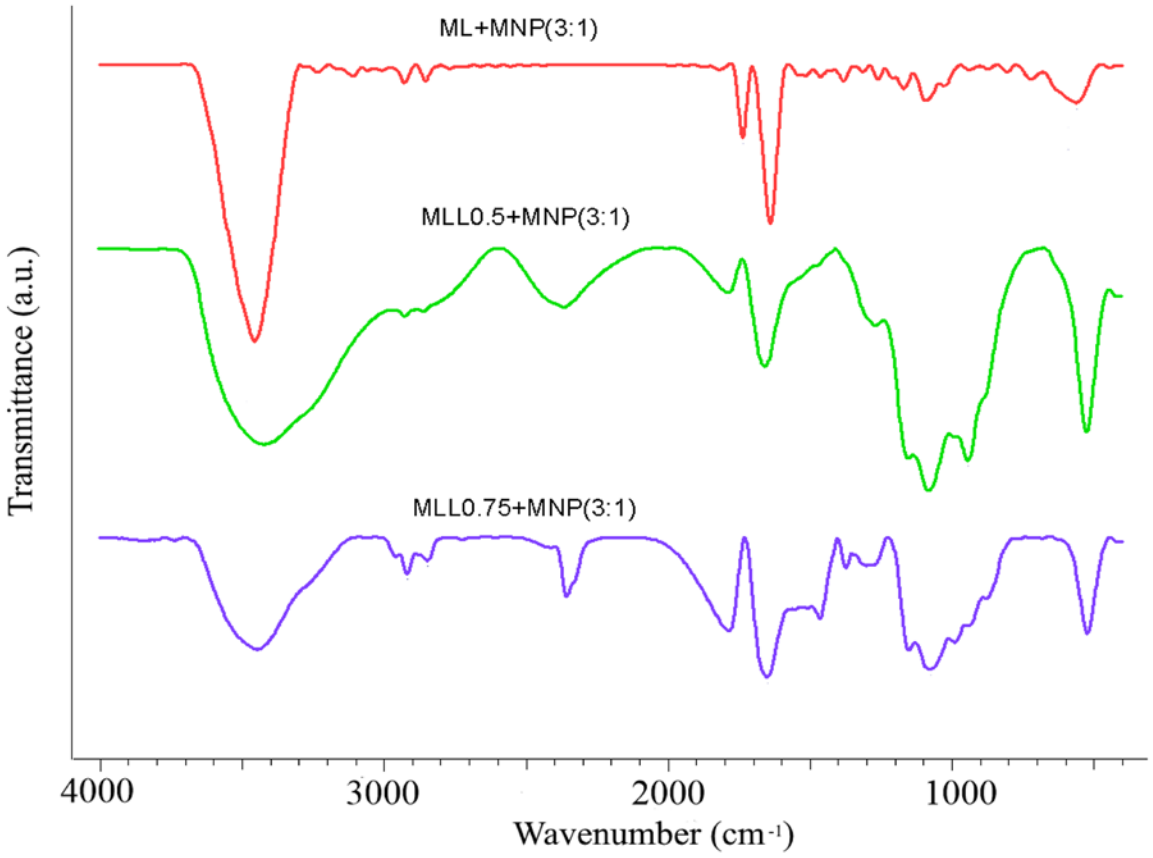

Fig. 7. FT-IR spectra for magnetic polymers and glyco-oligopeptides derivatives used in their preparation.

3.2.4. Characterization of the morphology of magnetic nanogels by the STEM technique

Based on the STEM images of the glyco-oligopeptides-coated MNPs shown in Fig. 8A, 8B and 8C, they are mostly spherical, with diameters ranging from 20 to 50 nm. In addition, a thin amorphous layer of glyco-oligopeptidess can be observed in all analyzed samples, which most likely incorporates several metal oxide nanoparticles in the cluster. When the glyco-oligopeptides consist of Leu only, a prominent aggregation of nanoparticles is observed, leading to the formation of large clusters. The degree of aggregation decreases with an increase in the proportion of Cbz-Lys added in the glyco-oligopeptides synthesis process, resulting in a smaller cluster of nanoparticles. As a result, Leu-rich formulations exhibit the most clustering effect, indicating that the absence of Cbz-Lys may reduce the capacity to stabilize the MNPs. In contrast, the improved dispersion and enhanced stabilization can be attributed to the potential hydrophobic or π-π stacking interactions between the Cbz radical and the MNPs.

The Cbz-Lys's steric hindrance, along with these interactions, is likely to explain the decreased aggregation of MNPs. Overall, the STEM images demonstrate that the coating affects the surface characteristics as well as the way the nanoparticles aggregate. The size, dispersion, and stability of the nanoparticle clusters may be controlled by varying the Leu/Cbz-Lys ratio, with the Cbz groups having an important effect in enhancing dispersion through compensatory/additional stabilizing forces like hydrophobic interactions or steric hindrance. This is consistent with the ZP trend that showed a decreasing ZP with the inclusion of Cbz-Lyz in the glyco-oligopeptides backbone due to a more shielded surface charge.

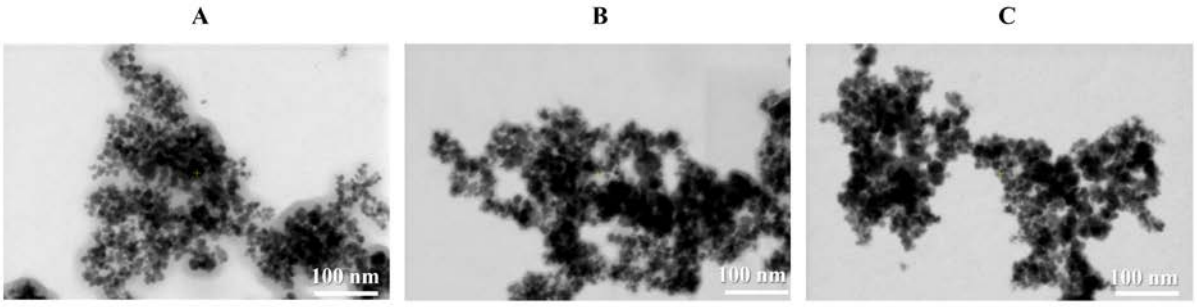

Fig. 8. A) STEM images for systems: ML+MNP(3:1), B) MLL0.5+MNP(3:1) and C) MLL0.75+MNP(3:1).

The size of the magnetic nanogels determined from the STEM technique is smaller than the one resulting from the DLS studies (Fig. 5B), because, upon drying, the electrostatic and hydrophobic interactions are reduced, causing the collapse of the nanogels' shell and the formation of clusters.

3.2.5. Magnetic susceptibility

The use of GOx-immobilized MNPs may constitute a potential dual treatment for melanoma. This approach combines the benefits of GOx enzymatic activity in glucose-rich tumoral tissues [27, 50] alongside magnetic propulsion to enhance the treatment efficiency. In this case, it is also important to investigate the magnetic properties of the new magnetic nanogels obtained by measuring the magnetic susceptibility after the assembly of MNPs with glyco-oligopeptidess.

The magnetic susceptibility data for colloidally dispersed (fluid) samples presented in Table 5 indicated a decrease in the magnetic susceptibility of the new magnetic nanogels compared to GOx-immobilized MNPs. This reduction may be attributed to magnetic dilution caused by dispersion in the buffer solution, as well as to the presence of the modified Cs layer grafted with oligopeptides, which reduce direct magnetic interactions between MNPs. Visual images of MLL0.5+MNP(3:1) were captured to demonstrate that, despite the low susceptibility values, the sample exhibits magnetic properties (see Fig. 9).

Table 5. Magnetic susceptibility data and DTIC loading capacity of synthesized magnetic nanogels.

Sample	Volumic magnetic susceptibility (χ_v) ($x10^{-8}$)	Volumic magnetisation (M_v) (emu/cm^3) ($x10^{-8}$)	DL (%)	EE (%)
MNP with GOx	130	58.5	-	-
ML+MNP(3:1)	30	13.5	69.52	26.25
MLL0.5+MNP(3:1)	7.4	3.33	62.60	22.34
MLL0.75+MNP(3:1)	2	0.9	58.35	19.94

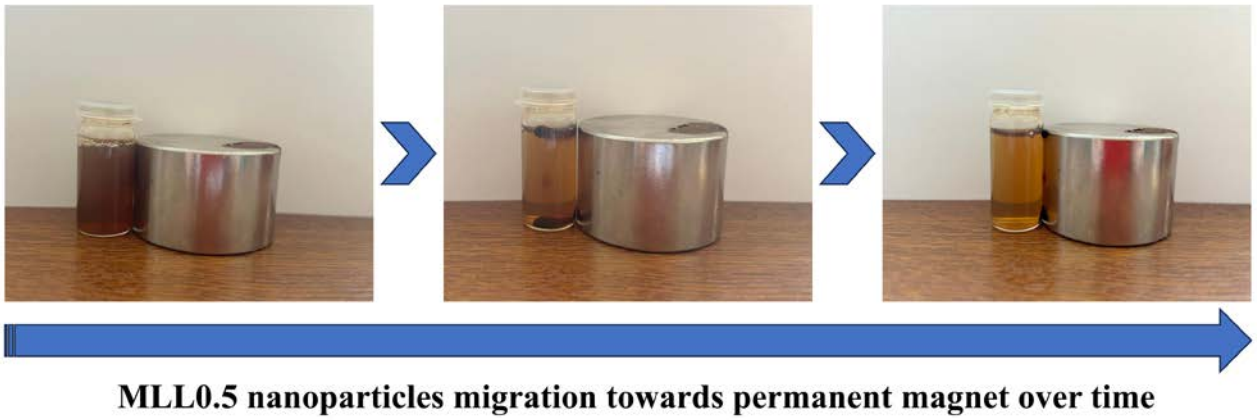

Fig. 9. Visual representation of remanent magnetisation of MLL0.5+MNP(3:1) sample over time.

As a result, the magnetic reactivity is maintained, but reduced, and not all nanogel particles are immediately attracted to the external magnet. The weak coloration of the magnetic nanogel suspension in Fig. 9 after the use of a permanent magnet does not indicate the absence of enzyme immobilization on the MNPs, but rather is a result of the reduced magnetic susceptibility and partial retention of the colloidal dispersion under the applied magnetic field. Although the glyco-oligopeptides coating reduced the magnetic susceptibility of MNPs immobilized with GOx, the good colloidal stability and small size of the nanoparticles will allow their movement to the desired areas (e.g. tumors).

Thus, the coating with polymers and GOx can influence the magnetic response by increasing the distance between the magnetic cores and limiting the effective alignment of the magnetic moments under the action of the applied external field. Moreover, the diamagnetic contribution of the glyco-oligopeptides shell can lower the magnetic susceptibility by inducing an additional shielding effect, although this is generally much weaker compared to the superparamagnetic influences of the nanoparticles [51]. This observation is in good agreement with previous studies in which a polymeric barrier reduced the magnetic susceptibility/magnetization of the core-shell MNPs [52].

3.2.6. Enzymatic activity

The inclusion of GOx-immobilized MNPs in self-assembled nanogels based on modified Cs grafted with oligopeptides significantly reduced the enzyme activity. This effect is attributed to the diffusion limitation of the glucose substrate through the polymer matrix, confirmed by the data obtained using the Trinder method of analysis.

It was also observed that the self-assembled nanogel shell, consisting of oligopeptide residues containing Leu and Cbz-Lys, leads to a decrease in the enzymatic activity of GOx. Specifically, the enzymatic activity dropped from 196.83 U/min for MNPs coated with the enzyme to 94.95, 69.48, and 21.91 U/min for magnetic nanogels ML+MNP (3:1), MLL0.5+MNP (3:1), and MLL0.75+MNP (3:1), respectively. This effect may be due to both the increase in hydrophobicity induced by Leu and Lys blocked with Cbz, and the compactness of the polymer layer, which may prevent the diffusion of water molecules and, implicitly, the glucose substrate, to the active sites of the enzyme, thereby inhibiting the formation of H_2O_2.

3.2.7. Propulsion tracking and MSD analysis of the magnetic nanogels

For the propulsion mechanism, glyco-oligopeptide nanogels containing GOx-MNPs were dispersed in a 10 mM glucose solution. Magnetic nanogels either with inactivated GOx or without the enzyme were prepared as controls; however, both formulations exhibited poor colloidal stability with the formation of aggregates, that not allow for a reliable tracking and comparison with the pristine magnetic nanogels, representing one of the limitations of this study (Tabel S2 and Fig. S3). Fig. 10 and related Videos 1-3 (from Supplementary Information) illustrate the motion of the magnetic nanogels, with the recorded time-lapse images showcasing the ability to visualize and track the propulsion dynamics simultaneously. It was observed that the catalytic GOx layer immobilized onto the MNPs, together with the surrounding glyco-oligopeptide-based shell containing the Leu/Cbz-Lys units, facilitates the efficient movement of the nanoparticles.

Thus, from the results it was observed a non-linear variation in propulsion speed influenced by the GOx activity as the Cbz-Lys grafting ratio increased: 4 μm/s (without Lys), 2.5 μm/s (1:0.5 mass ratio Leu/Cbz-Lys), and 8.9 μm/s (1:0.75 mass ratio Leu/Cbz-Lys). The sample with the highest Cbz-Lys ratio exhibited the fastest propulsion, whereas MLL0.5+MNP (3:1) was slower due to imbalanced hydrophobic–hydrophilic interactions that hindered optimal enzyme orientation. The measured velocities are comparable to those of enzyme-powered systems characterized in several research studies; therefore, a series of GOx/catalase-encapsulated nanomotors achieved peak

speeds of nearly 11.7 μm/s in 10 mM glucose solutions [53], whereas bubble-driven Janus micromotors reached speeds of up to 3 μm/s in a 10% H_2O_2 solution [54].

The motion of the new glyco-oligopeptide nanogels with a GOx-immobilized MNPs core is influenced by the GOx-powered self-diffusiophoresis, as was observed by other researchers characterizing a glucose-powered Janus nanomotor functionalized with GOx and polydopamine-Fe^{3+} chelates [55]. In this process, the localized catalytic conversion of glucose leads to the formation of concentration gradients of gluconic acid and H_2O_2 around the nanoparticle, inducing an interfacial fluid movement that allows the nanoparticles to self-propel. Thus, for the obtained magnetic nanogels, the enzymatic propulsion is aided by the MAC-g-oligo(Leu-co-Cbz-Lys) shell, which serves as a semipermeable interface that helps stabilize the chemical gradient.

Although the Lys units were introduced as N-carbobenzyloxy-protected NCA derivatives (Cbz-Lys-NCA), an increase in the grafted Cbz-Lys moieties was correlated with an improved catalytic propulsion of the nanogels. This effect suggests that the mechanisms responsible for the increased motility are not due to the electrical charge on the nanoparticle surface, as in the case of unblocked Lys units, but rather to the diffusion dynamics, GOx enzymatic activity, and hydrophobic–hydrophilic interactions between the nanogel shell and glucose substrate that induces a self-diffusiophoretic propulsion of the nanogels.

Regarding enzymatic activity, despite showing a significantly reduced residual enzymatic activity at the same glucose concentration (10 mM), the nanocarriers coated with modified Cs grafted with increasing Leu/Cbz-Lys ratio were characterized by an increased self-propulsion, a phenomenon correlated with the decrease in ZP (from +19 mV to +7.45 mV).

Thus, the observed dissociation between catalysis and velocities highlights that phoretic mobility, influenced by surface properties (hydrophobicity and aromatic interactions induced by Leu and Cbz-Lys sequences) and the modification of electric charge, is the primary parameter affecting the propulsion of the newly obtained magnetic nanogels. This aligns with the self-diffusiophoresis models, which state that the nanoparticle itself creates an asymmetric solutal concentration gradient, leading to the generation of a speed proportional to the product of the generated flux and surface mobility [56]. Gao et al.[57] reported in a research study on carbonaceous nanoflasks (CNF), that by modifying the surface properties (hydrophilic/hydrophobic), the phoretic mobility can be amplified through a locally produced glucose acid gradient independent of enzymatic activity.

Thus, short oligopeptide chains from the nanogels shell create a hydrophobic surface, causing a redistribution of the reaction towards the edges of the nanogels, which will favor the development of chemical gradients that promote self-propulsion. This highlights the importance of precise control over the composition of the peptide grafted onto the polysaccharide that forms the nanogel shell, as even slight changes in the amino acid sequence can affect the efficiency of catalytic propulsion.

Although the main conclusions of this analysis indicate a major influence of surface properties on nanogel mobility, since the control experiments that were conducted using magnetic nanogels without GOx or with inactive GOx were impossible to be used for a proper comparison of propulsion behavior, the influence of enzymatic activity cannot be completely separated from this observation, and as a result, it represents a limitation of the present study.

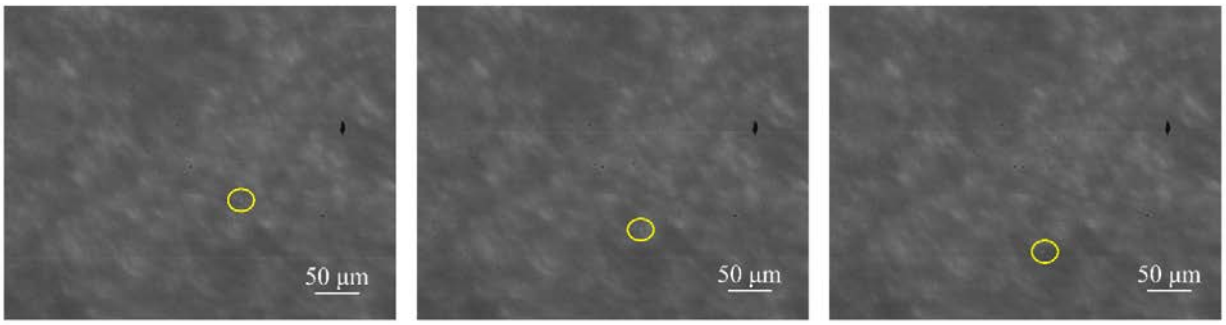

Fig. 10. Motion of self-propelled MLL0.75+MNP(3:1) nanogels in 10 mM glucose through optical snapshots from Supplementary Video 3 of nanogels moving at different times (1s, 2s and 3s, from left to right)

To improve the efficiency of drug delivery systems, evaluating diffusion parameters is essential because increased mobility improves tissue penetration, as observed in all prepared nanosystems. In this regard, to study the dynamics of the systems, the mean square displacements (MSDs) were investigated [58]. The particle trajectory was estimated by linking locations across frames and calculating the MSDs based on a random-walk model over a defined time scale.

Fig. 11 shows the MSD curves for the magnetic nanoparticle systems covered with the glyco-oligopeptide nanogel membrane (ML+MNP(3:1), MLL0.5+MNP(3:1) and MLL0.75+MNP(3:1)) as a function of the time interval Δt (lag time τ) in solution.

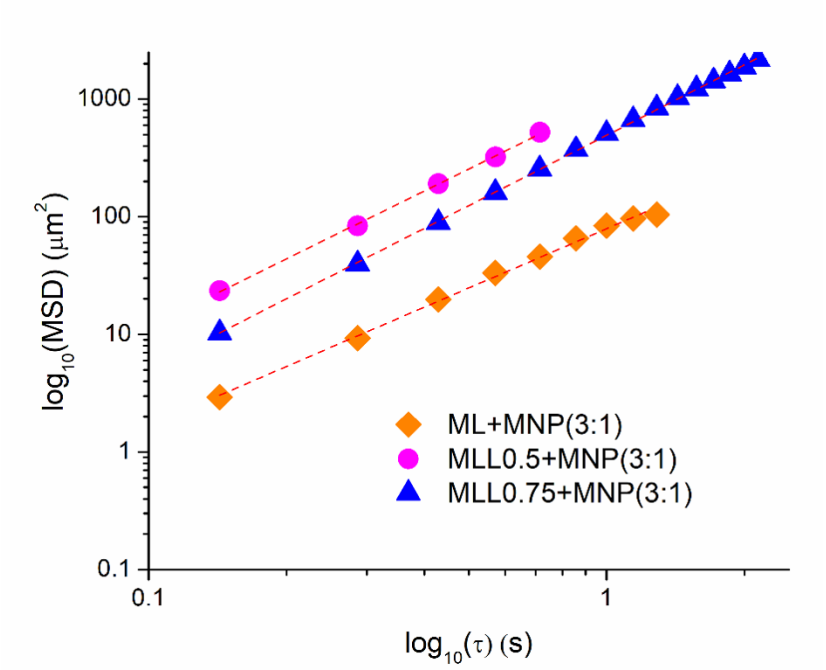

Fig. 11. Log-log plot of MSD of the magnetic glyco-oligopeptide-based nanogels as a function of lag time τ estimated from single-particle tracking.

We observed that all nanogels exhibited proportional increase in MSD, indicating superdiffusive motion based on the logarithmic slope of MSD versus time, with a value of $\alpha>1$, from 1.68 to 1.92 and 1.99 for ML+MNP(3:1), MLL0.5+MNP(3:1) and MLL0.75+MNP(3:1), respectively. This behavior is associated with a change in the hydrophilic-hydrophobic balance, which destabilizes the self-assembled nanogel shell and enhances mobility [59, 60].

Furthermore, the glyco-oligopeptide layer that stabilizes the MNPs has a major role in reducing uncontrolled mobility and dispersion of the magnetic nanogels outside the tumor area, facilitating their potential application in melanoma treatment.

3.2.8. Thermostability investigation

The influence of the glyco-oligopeptides composition on the thermal properties of the new magnetic nanogels was investigated by thermogravimetric analysis (TGA). The thermal parameters resulting from the TGA analysis of MNPs immobilized with enzymes, glyco-oligopeptidess containing Leu and Cbz-Lys and glyco-oligopeptidess-coated MNPs are summarized in Table 6. All glyco-oligopeptidess have, under 100°C, a weight loss of 3.57–8.03%,

which derives from water desorption. The thermal decomposition of ML, MLL0.5 and MLL0.75 took place in three stages, observing a gradual increase in the thermal stability due to the introduction of Cbz-Lys sequences into the structure of glyco-oligopeptidess. Moreover, the thermal analysis of MLL0.5 and MLL0.75 revealed decomposition temperatures for each stage larger than ML. The rigid aromatic units (Cbz) from the MLL0.5 and MLL0.75 glyco-oligopeptides chains have probably contributed to the high thermal stability in addition to the effect of the secondary polypeptidic structures organized by the intramolecular hydrogen bonds. The same observations were made for each glyco-oligopeptides-MNPs system, the thermostability increasing with the introduction of Cbz-Lys units due to the high bond dissociation energy of the aromatic ring structure. Similar observations were made by Ryu and colab. in the case of crystals based on Cbz-phenylalanine (Cbz-Phe) that had higher thermal stability (completely decomposing around 400 °C) and dense molecular packing [61].

Table 6. Parameters obtained following the TGA analysis of glyco-oligopeptidess, MNs and glyco-oligopeptidess/MNPs systems.

Sample	**Stage**	**T_{onset}**	**T_{peak}**	**W (%)**	**Residue (%)**
ML	I	29.8	66.8	8.03	34.31
	II	95.5	120	7.55	
	III	156.7	179.6	13.74	
	IV	201.0	218.3	36.37	
ML+MNP (3:1)	I	27.1	61.1	3.49	56.75
	II	143.5	161.4	4.02	
	III	218.3	245.2	9.5	
	IV	276.5	284	26.24	
MLL0.5	I	35.2	68.6	3.57	31.94
	II	107.7	161	13.01	
	III	200.5	224.4	38.33	

	IV	385.1	414.6	13.15	
MLL0.5+MNP (3:1)	I	28.6	60.7	1.6	55.64
	II	102.9	142	3.91	
	III	212.6	252	8.58	
	IV	260.2	288.1	30.27	
MLL0.75	I	29.7	61.3	7.67	25.44
	II	107.1	154.5	17.86	
	III	199.3	225.3	37.57	
	IV	367	413.7	11.46	
MLL0.75+MNP (3:1)	I	29.3	55.3	4.82	56.05
	II	110.1	162	3.35	
	III	218.7	244.3	10.29	
	IV	269.1	275.7	10.30	
	V	490.5	516.1	15.20	
MNP with GOx	I	32.9	127.9	4.3	78.1
	II	190.4	287.9	13.3	

3.2.9. In vitro drug loading and release experiments

Since the pH conditions in tumor tissues are frequently 0.5-1.0 units lower compared to healthy tissues as a result of glucose consumption and lactic acid accumulation, the evaluation of the release capacity of DTIC from the synthesized magnetic nanogels was carried out at two pH values, namely 6.5 and 7.4 [24]. The release study examines only the pH-dependent behavior of DTIC release from the magnetic nanogels, a key factor of the tumor microenvironment, highlighting that factors like GSH or enzymatic remodeling will be explored in future investigations to gain a comprehensive understanding of the nanogels' behaviour.

The release study examines behavior that is influenced by pH, a key feature of the tumor microenvironment. Additional elements like GSH or enzymatic remodeling were not explored and are recognized as areas for future research.

To quantify the drug loading efficiency, both EE% and DL% were calculated for the DTIC-loaded magnetic nanogels and the corresponding results are listed in Table 4 above.

Overall, *in vitro* drug release shows a two-phase pattern comprising an initial rapid release followed by sustained slow release over an extended period lasting up to 48 hours (see Fig. 8). The drug releases gradually, most likely due to the glyco-oligopeptides layer dissociating from the iron oxide core.

The cumulative release of DTIC from the magnetic nanogels slightly increased as the pH decreased from pH 7.4 to 6.5 (Fig. 12). In addition, at both pHs, the ML+MNP(3:1) nanoparticles loaded with DTIC had the lowest release rates compared to MLL0.5+MNP(3:1) and MLL0.75+MNP(3:1) loaded with DTIC, behavior that can be associated with the drug-glyco-oligopeptides shell interactions. This observation correlates with the EE% values, which were lower for the MLL0.5+MNP(3:1) (22.34%) and MLL0.75+MNP(3:1) (19.94%) systems compared to the ML+MNP(3:1) sample (26.25%). The ML nanoparticles are more compact, which allows the incorporation of a relatively larger amount of drug. It was found that approximately 63.83%, 87.19% and 93.55% of DTIC loaded in samples ML+MNP(3:1), MLL0.5+MNP(3:1) and MLL0.75+MNP(3:1), respectively, were released in 24 hours in the simulated tumour microenvironment (pH 6.5). It is most likely that the drug-nanogels interactions were diminished by the electrostatic forces of repulsion between the positively charged DTIC molecules and the glyco-oligopeptides network.

Although there were only minor differences regarding DTIC release across the studied pHs, DTIC molecules can be discharged from these magnetic nanogels at a controlled rate in melanoma therapy due to the acidic microenvironment found in intracellular lysosomes or endosomes within cancer cells.

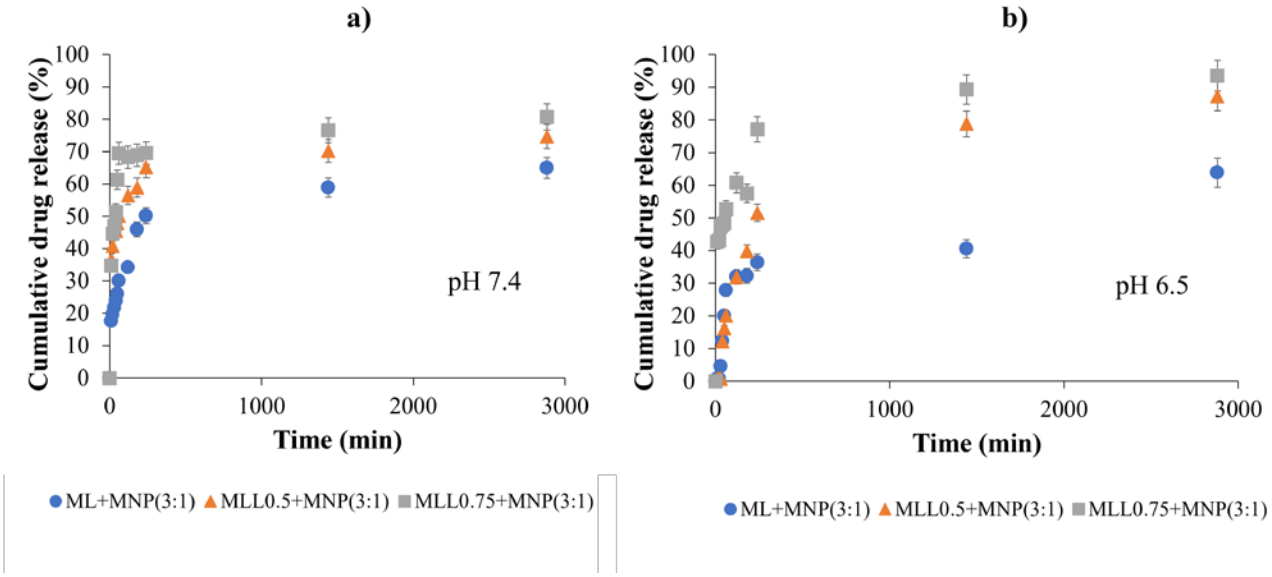

Fig. 12. Graphical representation of DTIC release from magnetic nanogels over time at a) pH 7.4 and b) pH 6.5.

3.2.10. Assessment of cytotoxicity of nanogels (MTS assay)

To assess the impact of pristine nanogels (ML+MNP(3:1), MLL0.5+MNP(3:1) and MLL0.75+MNP(3:1)) or those loaded with DTIC on cell viability, melanocytes and fibroblast cells were exposed to varying concentrations (175–292 µg/mL) of each type of magnetic nanogel with or without DTIC for 24h. Pairwise comparisons between formulations at each concentration were performed using a two-tailed Student's t-test (n = 3, dl = 4). No direct comparisons were made between empty nanogels and free DTIC, as they have a different mechanism of action on cells. No pronounced dose-dependent cytotoxicity on normal fibroblast was observed within the tested concentration range for pristine magnetic nanogels, namely ML+MNP(3:1), MLL0.5+MNP(3:1) and MLL0.75+MNP(3:1) (Fig. 13A). Specifically, at 175 µg/mL, statistical analysis revealed no significant differences between tested formulations ($p>0.05$), indicating similar cytocompatibility at this concentation. At 233 µg/mL, ML+MNP(3:1) had significantly higher viability than MLL0.5+MNP(3:1) ($p<0.05$), but no difference was observed between ML+MNP(3:1) and MLL0.75+MNP(3:1) ($p = 0.331$). MLL0.5+MNP(3:1) and MLL0.75+MNP(3:1) showed a significant difference ($p<0.01$). At the highest tested concentration (292 µg/mL), although all

formulations differed significantly ($p < 0.01$), cell viability remained above 90% in each case, supporting their good cytocompatibility.

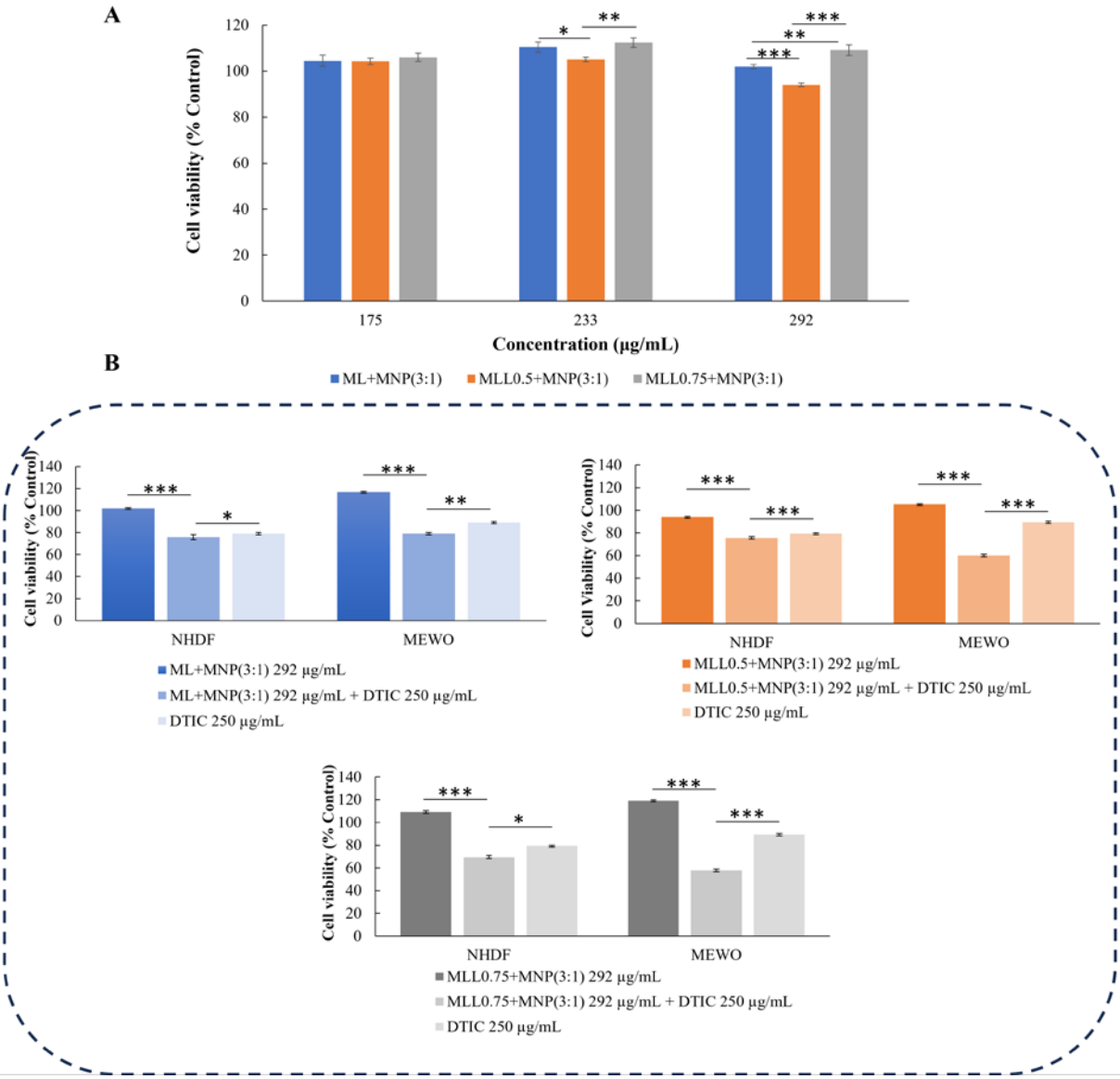

Fig. 13. A) Viability of normal fibroblasts after 24h incubation with nanoparticles (175, 233, 292 µg/mL); B)Viability of normal fibroblasts (NHDF) and malignant melanoma cells (MeWo) after 24h incubation with magnetic nanogels, nanogels loaded with DTIC or free DTIC. The differences between ML+MNP(3:1), MLL0.5+MNP(3:1) and MLL0.75+MNP(3:1) at the same concentration were compared statistically. Values represent mean ± SD (n = 3), *$p \leq 0.05$, **$p \leq 0.01$, ***$p \leq 0.001$.

Nanogels loaded with DTIC were not cytotoxic for normal fibroblasts at the tested concentrations (292 µg/mL for nanoparticles and 250 µg/mL for DTIC), but they determined cytotoxic effects on malignant melanoma cells (Fig. 13B). Thus, ML+MNP(3:1)_DTIC determined the decrease of MeWo viability to 79%, MLL0.5+MNP(3:1)_DTIC to 60%, and MLL0.75+MNP(3:1)_DTIC to 58% and, over time, the viability of normal fibroblasts remained higher than 70% (Fig. 13B). Also, magnetic nanogels loaded with DTIC, particularly at the highest tested dose, determined stronger cytotoxic effects on malignant melanoma cells compared to free DTIC (89%) at the same concentration. For ML+MNP(3:1)_DTIC, the cytotoxicity of loaded magnetic nanogels versus free DTIC was significant (*$p<0.01$). In contrast, for MLL0.5+MNP(3:1)_DTIC and MLL0.75+MNP(3:1)_DTIC, highly significant differences were observed (**$p<0.001$), suggesting improved enhanced antitumoral efficacy, particularly for the higher Cbz-Lys-containing systems.

Although cytotoxicity testing was conducted with a 24-hour exposure period, using concentrations up to 292 µg/mL for bare magnetic nanogels and 250 µg/mL for DTIC, these initial results suggest a promising safety profile. Extending testing to higher doses and longer durations to evaluate any delayed or cumulative toxicity will be the subject of further studies.

3.2.11. Assessment of in vivo biocompatibility

The *in vivo* study shows short-term biocompatibility after subcutaneous administration of ML and MNP(3:1) samples, and therefore, long-term biodistribution and organ will be investigated in future studies.

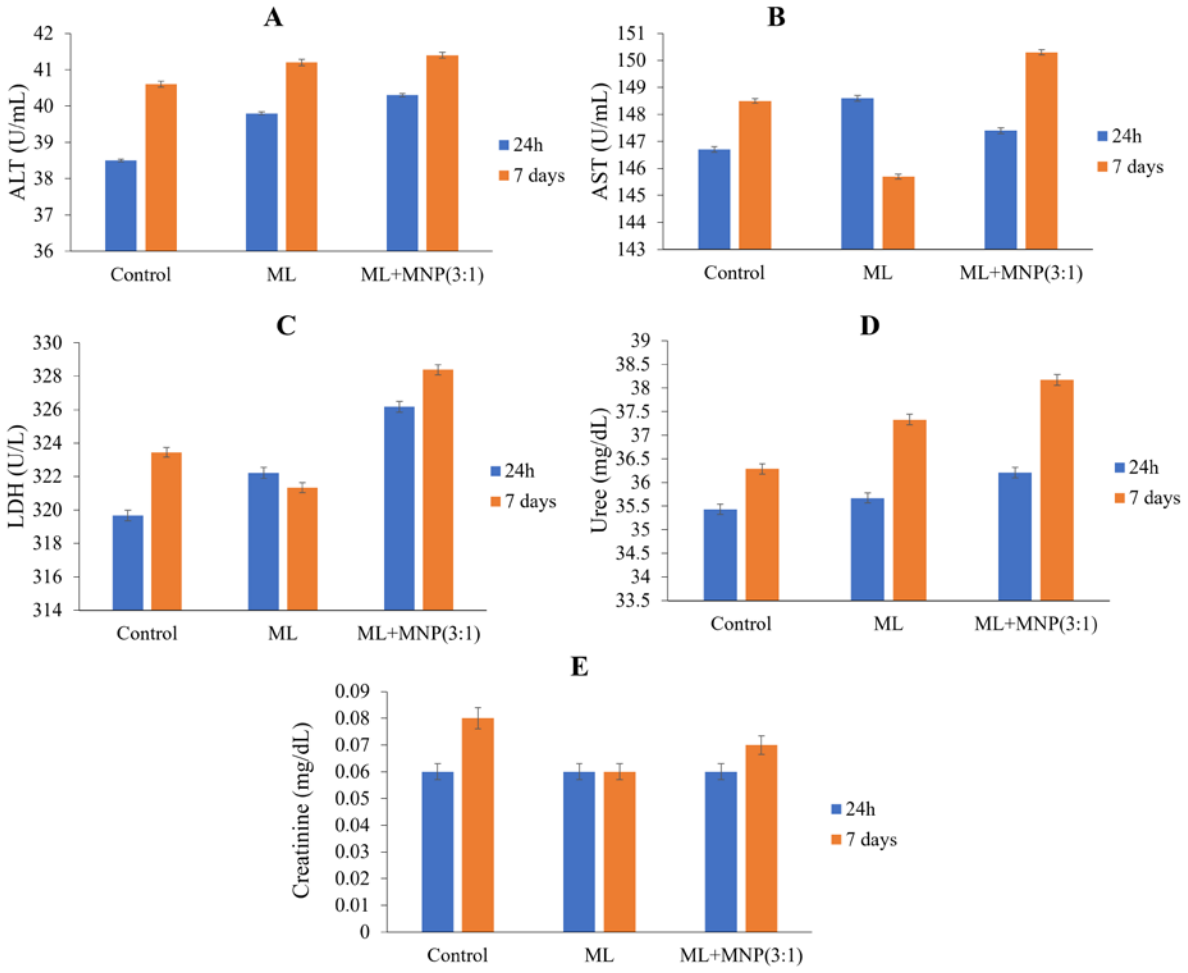

Fig. 14. ML and ML+MNP(3:1) effects on ALT, AST, LDH activity, blood urea and creatinine levels. Values are expressed as mean ± S.D. for 6 rats per lot.

The data obtained indicated that there were no statistically significant changes in the number of erythrocytes (GR), hemoglobin (Hb), and hematocrit (Ht) values in the animals that received P and PMNP, compared to the animals in the control group, at 24 hours or 7 days in the experiment (which are presented in the Supporting Information material of this study – Fig. S5)

The analysis of the leukocyte formula highlighted that in the animal groups that received ML and ML+MNP(3:1), the percentage values of polymorphonuclear neutrophils (PMN, lymphocyte (Ly), eosinophils (E), monocytes (M), basophils (B) elements are at similar levels to those of the control animals, at both times of the investigations (Fig. S6 from the Supporting Information, Section S6).

The measurement of the activity of liver enzymes showed no significant differences in the levels of ALT, AST and LDH in the blood between the groups that received ML and ML+MNP(3:1),

compared to the group with distilled water, 24 hours and 7 days after administering the tested substances. Overall, these results indicate that the materials did not induce hepatocyte alterations or liver dysfunction (Fig. 14).

The subcutaneous injection of ML and ML+MNP(3:1) did not produce substantial variations in the plasma levels of urea and creatinine compared to the control group at both time intervals in the experiment (Fig. 14), indicating no kidney dysfunction.

No statistically significant changes were noted in the activity of serum complement and the phagocytosis capacity of PMN from the peripheral blood between the animals in the groups with ML, respectively ML+MNP(3:1) and the animals that received distilled water at 24 hours and 7 days (Fig. S7a). This observation suggests that the tested nanogels do not induce an immune response, which is essential for their safe use in biomedical applications.

The use of ML and ML+MNP(3:1) was not accompanied by obvious variations in the serum values of IL-6 and TNFα compared to the control group, at both times of the determinations (Fig. S7e and S7f).

The determination of serum complement fractions did not show considerable differences between C3 and C4 values in the animals treated with ML, respectively with ML+MNP(3:1) and the animals that were administered distilled water after 24 hours and 7 days in the experiment (Fig. S7b and S7c).

We concluded that, following subcutaneous administration of the tested magnetic nanogels to mice, with or without DTIC, similar hematological, biochemical and immune responses were observed that were comparable to those of the control group, indicating good in vivo biocompatibility. These findings, together with the observed biodegradability of the compound, confirmed through enzymatic assay (see Supporting Information, Section S5), support the potential suitability of glyco-oligopeptides-coated nanomotor systems containing GOx-immobilized MNPs as DTIC delivery systems in therapeutic applications for melanoma.

Conclusions

In this study, self-propelled magnetic nanogels loaded with DTIC were succefully developed via the supramolecular assembly of novel glyco-oligopeptidess and enzyme-conjugated MNPs for use in melanoma therapy. The glyco-oligopeptidess were synthesized by ROP of Leu-NCA and Cbz-Lys-NCA using the unreacted amino groups from Cs functionalized with MA. The FT-IR and ^{1}H

NMR analyses confirmed the ring opening of the NCA-amino acids and grafting to MAC. The MNPs were successfully synthesized via the co-precipitation method and conjugated with GOx through Schiff base formation.

DLS studies indicated that magnetic nanogels coated with MLL0.5 or MLL0.75 had higher average sizes and lower ZP values (+7.26 mV to +7.68 mV) compared to ML+MNP(3:1), attributed to hydrophobic polypeptidic chains with Cbz-Lys units shielding surface charges.

Particle tracking and MSD assays revealed a superdiffusive motion for all systems with Cbz-Lys-rich glyco-oligopeptides displaying the highest speed up to 8.9 μm/s.

The in vitro drug release tests of magnetic nanogels encapsulating DTIC demonstrated a pH-responsive behavior influenced by the glyco-oligopeptides composition, showing a two-phase release pattern: a rapid initial release followed by a gradual one lasting up to 48 hours due to the glyco-oligopeptides layer detachment from the iron oxide core. Moreover, the combination of Leu and Cbz-Lys in the glyco-oligopeptide shell provided better protection against lysozyme degradation (as detailed in the Supporting Information in Section S).

The systems demonstrated a decrease in cytotoxicity on fibroblasts while showing high efficacy against melanocytes compared to non-encapsulated DTIC. In vivo experiments on laboratory animals indicated good hemocompatibility of the magnetic polymers (detailed in Supporting Information, Section S7), without adverse effects on liver and kidney tissues both of which are involved in the elimination of MNPs through phagocytosis.

Overall, the results of the present study support the initial hypothesis that glyco-oligopeptides/GOx-MNPs-based nanogels can effectively serve as advanced nanocarriers for DTIC, enhancing cytotoxicity toward melanocytes.

Declaration of competing interest

The authors declare that they have no known competing financial interests or personal relationships that could have appeared to influence the work reported in this paper.

Acknowledgement

This research is carried out and financed within the framework of the Second Swiss Contribution MAPS (project code: F-RO-CH-2024-0081).

CRediT authorship contribution statement

Alina Gabriela Rusu: Conceptualization, Methodology, Validation, Formal analysis, Investigation, Writing – original draft, Visualization. **Loredana Elena Niță**: Methodology, Investigation, Writing – review & editing, Supervision. **Alina Ghilan**: Investigation, Writing – original draft, Visualization. **Natalia Simionescu**: Methodology, Validation, Formal analysis, Investigation,Writing – original draft. **Alexandru-Mihail Șerban**: Methodology, Validation, Formal analysis, Writing – review & editing. **Alexandra Vieru**: Methodology, Validation, Formal analysis, Writing – review & editing. **Liliana Mititelu-Tarțău**: Methodology, Validation, Formal analysis, Investigation,Writing – original draft.

Declaration of generative AI and AI-assisted technologies in the writing process

During the preparation of this work the author(s) used Grammarly in order to improve language and readability. After using this tool, the author(s) reviewed and edited the content as needed and take(s) full responsibility for the content of the publication.

References

[1] Z. Cheng, M. Li, R. Dey, Y. Chen, Nanomaterials for cancer therapy: current progress and perspectives, Journal of Hematology & Oncology 14(1) (2021) 85.
[2] Z. Cheng, M. Li, R. Dey, Y. Chen, Nanomaterials for cancer therapy: current progress and perspectives, Journal of hematology & oncology 14(1) (2021) 85.
[3] S. Vankudre, N. Shirkoli, R. Hawaldar, H. Shetti, Enhanced delivery of Dacarbazine using Nanosponge loaded Hydrogel for Targeted Melanoma Treatment: Formulation, Statistical Optimization and Pre-clinical Evaluation, Journal of Pharmaceutical Innovation 20(1) (2025) 27.
[4] S.B. Lee, J.M. Park, R. Park, H.E. Choi, S.W. Hong, K.S. Kim, Synergistic chemo-photothermal treatment via MXene-encapsulated nanoparticles for targeted melanoma therapy, Journal of Controlled Release 382 (2025) 113729.
[5] L.A. Jadhav, S.K. Mandlik, Nanocarriers in skin cancer treatment: Emerging drug delivery approaches and innovations, Nano TransMed 4 (2025) 100068.
[6] L. Blagojevic, N. Kamaly, Nanogels: A chemically versatile drug delivery platform, Nano Today 61 (2025) 102645.
[7] B. Wang, S. Hu, Y. Teng, J. Chen, H. Wang, Y. Xu, K. Wang, J. Xu, Y. Cheng, X. Gao, Current advance of nanotechnology in diagnosis and treatment for malignant tumors, Signal Transduction and Targeted Therapy 9(1) (2024) 200.
[8] L. Radeva, K. Yoncheva, Nanogels—Innovative Drug Carriers for Overcoming Biological Membranes, 11(2) (2025) 124.
[9] M.U. Munir, Nanomedicine Penetration to Tumor: Challenges, and Advanced Strategies to Tackle This Issue, Cancers 14(12) (2022).
[10] Y. Qin, P. Li, Antimicrobial Chitosan Conjugates: Current Synthetic Strategies and Potential Applications, International journal of molecular sciences 21(2) (2020).

[11] U.K. Biswas, A. Bose, B. Ghosh, S. Sharma, An insight into chemically modified chitosan and their biological, pharmaceutical, and medical applications: A review, International Journal of Biological Macromolecules 303 (2025) 140612.
[12] A.G. Rusu, A.P. Chiriac, L.E. Nita, I. Rosca, M. Pinteala, L. Mititelu-Tartau, Chitosan Derivatives in Macromolecular Co-assembly Nanogels with Potential for Biomedical Applications, Biomacromolecules 21(10) (2020) 4231-4243.
[13] H. Omidian, L.X. Cubeddu, R.L. Wilson, Peptide-Functionalized Nanomedicine: Advancements in Drug Delivery, Diagnostics, and Biomedical Applications, 30(7) (2025) 1572.
[14] S.M.P. Vadevoo, S. Gurung, H.-S. Lee, G.R. Gunassekaran, S.-M. Lee, J.-W. Yoon, Y.-K. Lee, B. Lee, Peptides as multifunctional players in cancer therapy, Experimental & Molecular Medicine 55(6) (2023) 1099-1109.
[15] C.A. Allred, C. Gormley, I. Venugopal, S. Li, M.J. McGuire, K.C. Brown, Tumor-specific intracellular delivery: peptide-guided transport of a catalytic toxin, Communications biology 6(1) (2023) 60.
[16] X. Chen, Z. Zhao, K.V. Laster, K. Liu, Z. Dong, Advancements in therapeutic peptides: Shaping the future of cancer treatment, Biochimica et Biophysica Acta (BBA) - Reviews on Cancer 1879(6) (2024) 189197.
[17] S. O'Flaherty, O.A. Luzina, N.S. Dyrkheeva, Y. Krier, J. Leprince, A.L. Zakharenko, M.A. Pokrovsky, A.G. Pokrovsky, O.I. Lavrik, N.F. Salakhutdinov, M. Varbanov, M. Devocelle, K.P. Volcho, Novel Peptide–Drug Conjugates with Dual Anticancer Activity, 25(22) (2024) 12411.
[18] V. Castelletto, J. Seitsonen, J. Ruokolainen, C. Piras, R. Cramer, C.J.C. Edwards-Gayle, I.W. Hamley, Peptide nanotubes self-assembled from leucine-rich alpha helical surfactant-like peptides, Chemical Communications 56(80) (2020) 11977-11980.
[19] M. Zheng, M. Pan, W. Zhang, H. Lin, S. Wu, C. Lu, S. Tang, D. Liu, J. Cai, Poly(α-l-lysine)-based nanomaterials for versatile biomedical applications: Current advances and perspectives, Bioactive Materials 6(7) (2021) 1878-1909.
[20] G.L. Eakins, J.K. Gallaher, R.A. Keyzers, A. Falber, J.E.A. Webb, A. Laos, Y. Tidhar, H. Weissman, B. Rybtchinski, P. Thordarson, J.M. Hodgkiss, Thermodynamic Factors Impacting the Peptide-Driven Self-Assembly of Perylene Diimide Nanofibers, The Journal of Physical Chemistry B 118(29) (2014) 8642-8651.
[21] F. Santino, P. Stavole, T. He, S. Pieraccini, M. Paolillo, L. Prodi, E. Rampazzo, L. Gentilucci, Preparation of Non-Toxic Fluorescent Peptide-Coated Silica/PEG Nanoparticles from Peptide-Block Copolymer Conjugates, 2(2) (2022) 240-256.
[22] T.P. Enright, D.L. Garcia, G. Storti, J.E. Heindl, A. Sidorenko, Synthesis and Antibiotic Activity of Chitosan-Based Comb-like Co-Polypeptides, 21(4) (2023) 243.
[23] D. Lu, H. Wang, X. Wang, Y. Li, H. Guo, S. Sun, X. Zhao, Z. Yang, Z. Lei, Biomimetic chitosan-graft-polypeptides for improved adhesion in tissue and metal, Carbohydrate polymers 215 (2019) 20-28.
[24] Q. He, J. Chen, J. Yan, S. Cai, H. Xiong, Y. Liu, D. Peng, M. Mo, Z. Liu, Tumor microenvironment responsive drug delivery systems, Asian journal of pharmaceutical sciences 15(4) (2020) 416-448.
[25] K.M. Abdullah, G. Sharma, A.P. Singh, J.A. Siddiqui, Nanomedicine in Cancer Therapeutics: Current Perspectives from Bench to Bedside, Molecular cancer 24(1) (2025) 169.
[26] S. Liu, Z. Ren, M. Yan, W. Ye, Y. Hu, Strategies to enhance the penetration of nanomedicine in solid tumors, Biomaterials 321 (2025) 123315.
[27] S. Li, Q. Wang, Z. Jia, M. Da, J. Zhao, R. Yang, D. Chen, Recent advances in glucose oxidase-based nanocarriers for tumor targeting therapy, Heliyon 9(10) (2023) e20407.
[28] J. Bhoopathy, S.W. Vedakumari, Y.R. Pravin, A.D. Prabhu, A. Robert, Synthesis and characterization of sericin-based magnetic nanoparticles for MR imaging application - An in vivo study, International Journal of Biological Macromolecules 310 (2025) 143415.
[29] W. Graham, M. Torbett-Dougherty, A. Islam, S. Soleimani, T.A. Bruce-Tagoe, J.A. Johnson, Magnetic Nanoparticles and Drug Delivery Systems for Anti-Cancer Applications: A Review, 15(4) (2025) 285.

[30] A.G. Rusu, A.P. Chiriac, L.E. Nita, M. Bercea, N. Tudorachi, A. Ghilan, D. Pamfil, D. Rusu, F.D. Cojocaru, Interpenetrated polymer network with modified chitosan in composition and self-healing properties, International Journal of Biological Macromolecules 132 (2019) 374-384.
[31] Y. Wu, K. Chen, J. Wang, M. Chen, W. Dai, R. Liu, Recent Advances and Future Developments in the Preparation of Polypeptides via N-Carboxyanhydride (NCA) Ring-Opening Polymerization, Journal of the American Chemical Society 146(35) (2024) 24189-24208.
[32] V. Balan, G. Dodi, N. Tudorachi, O. Ponta, V. Simon, M. Butnaru, L. Verestiuc, Doxorubicin-loaded magnetic nanocapsules based on N-palmitoyl chitosan and magnetite: Synthesis and characterization, Chemical Engineering Journal 279 (2015) 188-197.
[33] A.G. Rusu, A.P. Chiriac, L.E. Nita, V. Balan, A.M. Serban, A. Croitoriu, Synthesis and Comparative Studies of Glucose Oxidase Immobilized on Fe3O4 Magnetic Nanoparticles Using Different Coupling Agents, 12(14) (2022) 2445.
[34] G.K. Kouassi, J. Irudayaraj, G. McCarty, Activity of glucose oxidase functionalized onto magnetic nanoparticles, Biomagnetic research and technology 3(1) (2005) 1.
[35] X. Ma, A. Jannasch, U.-R. Albrecht, K. Hahn, A. Miguel-López, E. Schäffer, S. Sánchez, Enzyme-Powered Hollow Mesoporous Janus Nanomotors, Nano Letters 15(10) (2015) 7043-7050.
[36] C. Schirripa Spagnolo, S. Luin, Trajectory Analysis in Single-Particle Tracking: From Mean Squared Displacement to Machine Learning Approaches, 25(16) (2024) 8660.
[37] J.R. Clegg, A.S. Irani, E.W. Ander, C.M. Ludolph, A.K. Venkataraman, J.X. Zhong, N.A. Peppas, Synthetic networks with tunable responsiveness, biodegradation, and molecular recognition for precision medicine applications, Science advances 5(9) (2019) eaax7946.
[38] A.K. Sharma, P. Prasher, A.A. Aljabali, V. Mishra, H. Gandhi, S. Kumar, S. Mutalik, D.K. Chellappan, M.M. Tambuwala, K. Dua, D.N. Kapoor, Emerging era of “somes”: polymersomes as versatile drug delivery carrier for cancer diagnostics and therapy, Drug Delivery and Translational Research 10(5) (2020) 1171-1190.
[39] I. Greco, N. Molchanova, E. Holmedal, H. Jenssen, B.D. Hummel, J.L. Watts, J. Håkansson, P.R. Hansen, J. Svenson, Correlation between hemolytic activity, cytotoxicity and systemic in vivo toxicity of synthetic antimicrobial peptides, Scientific Reports 10(1) (2020) 13206.
[40] Directive 2010/63/EU of the European Parliament and of the Council of 22 September 2010 on the protection of animals used for scientific purposes, 2010. https://eur-lex.europa.eu/legal-content/EN/LSU/?uri=oj:JOL_2010_276_R_NS004. (Accessed 04/10 2024).
[41] A.G. Rusu, M.I. Popa, C. Ibanescu, M. Danu, L. Verestiuc, Tailoring the properties of chitosan-poly(acrylic acid) based hydrogels by hydrophobic monomer incorporation, Materials Letters 164 (2016) 320-324.
[42] H.A. Mohamed, M. Khuphe, S.J. Boardman, S. Shepherd, R.M. Phillips, P.D. Thornton, C.E. Willans, Polymer encapsulation of anticancer silver–N-heterocyclic carbene complexes, RSC Advances 8(19) (2018) 10474-10477.
[43] C. Park, J.-W. Lim, G. Park, H.-O. Kim, S. Lee, Y.H. Kwon, S.-E. Kim, M. Yeom, W. Na, D. Song, E. Kim, S. Haam, Kinetic stability modulation of polymeric nanoparticles for enhanced detection of influenza virus via penetration of viral fusion peptides, Journal of Materials Chemistry B 9(47) (2021) 9658-9669.
[44] J. Stulz, D. Müller, W.E. Hull, H.R. Kricheldorf, Secondary structure of peptides, 10. FT-IR and 13C NMR CP/MAS study on tacticity and secondary structure of poly(D,L-leucine)s, 184(6) (1983) 1311-1322.
[45] D. Pranantyo, L.Q. Xu, Z. Hou, E.-T. Kang, M.B. Chan-Park, Increasing bacterial affinity and cytocompatibility with four-arm star glycopolymers and antimicrobial α-polylysine, Polymer Chemistry 8(21) (2017) 3364-3373.
[46] M. Kaliva, A. Georgopoulou, D.A. Dragatogiannis, C.A. Charitidis, M. Chatzinikolaidou, M. Vamvakaki, Biodegradable Chitosan-graft-Poly(l-lactide) Copolymers For Bone Tissue Engineering, 12(2) (2020) 316.

[47] R. Bucci, D. Maggioni, S. Locarno, A.M. Ferretti, M.L. Gelmi, S. Pellegrino, Exploiting Ultrashort α,β-Peptides in the Colloidal Stabilization of Gold Nanoparticles, Langmuir 37(38) (2021) 11365-11373.
[48] E.A. Egorova, M.M.J. van Rijt, N. Sommerdijk, G.S. Gooris, J.A. Bouwstra, A.L. Boyle, A. Kros, One Peptide for Them All: Gold Nanoparticles of Different Sizes Are Stabilized by a Common Peptide Amphiphile, ACS Nano 14(5) (2020) 5874-5886.
[49] J. Niu, M. Yuan, Y. Liu, L. Wang, Z. Tang, Y. Wang, Y. Qi, Y. Zhang, H. Ya, Y. Fan, Silk peptide-hyaluronic acid based nanogels for the enhancement of the topical administration of curcumin, Volume 10 - 2022 (2022).
[50] J.A. Stinson, A. Sheen, B.M. Lax, G.N. Yang, L. Duhamel, L. Santollani, E. Fink, J.R. Palmeri, K.D. Wittrup, Tumor Integrin-Targeted Glucose Oxidase Enzyme Promotes ROS-Mediated Cell Death that Combines with Interferon Alpha Therapy for Tumor Control, Molecular cancer therapeutics 24(1) (2025) 118-130.
[51] C. Cruzat Contreras, O. Peña, M.F. Meléndrez, J. Díaz-Visurraga, G. Cárdenas, Synthesis, characterization and properties of magnetic colloids supported on chitosan, Colloid and Polymer Science 289(1) (2011) 21-31.
[52] N. Cruz, J.O. Pinho, G. Soveral, L. Ascensão, N. Matela, C. Reis, M.M. Gaspar, A Novel Hybrid Nanosystem Integrating Cytotoxic and Magnetic Properties as a Tool to Potentiate Melanoma Therapy, 10(4) (2020) 693.
[53] B.J. Toebes, F. Cao, D.A. Wilson, Spatial control over catalyst positioning on biodegradable polymeric nanomotors, Nature Communications 10(1) (2019) 5308.
[54] J. Shao, S. Cao, H. Che, M.T. De Martino, H. Wu, L.K.E.A. Abdelmohsen, J.C.M. van Hest, Twin-Engine Janus Supramolecular Nanomotors with Counterbalanced Motion, Journal of the American Chemical Society 144(25) (2022) 11246-11252.
[55] Y. Ji, Y. Pan, X. Ma, Y. Ma, Z. Zhao, Q. He, pH-Sensitive Glucose-Powered Nanomotors for Enhanced Intracellular Drug Delivery and Ferroptosis Efficiency, Chemistry, an Asian journal 19(1) (2024) e202300879.
[56] N. Sharifi-Mood, J. Koplik, C. Maldarelli, Diffusiophoretic self-propulsion of colloids driven by a surface reaction: The sub-micron particle regime for exponential and van der Waals interactions, Physics of Fluids 25(1) (2013).
[57] C. Gao, C. Zhou, Z. Lin, M. Yang, Q. He, Surface Wettability-Directed Propulsion of Glucose-Powered Nanoflask Motors, ACS Nano 13(11) (2019) 12758-12766.
[58] R.P. Mohanty, X. Liu, J.Y. Kim, X. Peng, S. Bhandari, J. Leal, D. Arasappan, D.C. Wylie, T. Dong, D. Ghosh, Identification of peptide coatings that enhance diffusive transport of nanoparticles through the tumor microenvironment, Nanoscale 11(38) (2019) 17664-17681.
[59] R.V. Ulijn, A.M. Smith, Designing peptide based nanomaterials, Chemical Society Reviews 37(4) (2008) 664-675.
[60] X. Yan, P. Zhu, J. Li, Self-assembly and application of diphenylalanine-based nanostructures, Chemical Society Reviews 39(6) (2010) 1877-1890.
[61] J. Ryu, C.B. Park, High-Temperature Self-Assembly of Peptides into Vertically Well-Aligned Nanowires by Aniline Vapor, 20(19) (2008) 3754-3758.